Clim Dyn (2015) 45:1471–1492
DOI 10.1007/s00382-014-2397-9

Impact of interactive vegetation phenology on the Canadian RCM simulated climate over North America

Camille Garnaud · Laxmi Sushama · Diana Verseghy

Received: 23 April 2014 / Accepted: 1 November 2014 / Published online: 12 November 2014

Abstract Biosphere–atmosphere interactions play a very important role in modulating regional climate. To capture these bi-directional interactions, a dynamic vegetation model, the Canadian Terrestrial Ecosystem Model (CTEM), has been implemented in the fifth generation of the Canadian Regional Climate Model (CRCM5). CTEM can grow vegetation from bare ground and includes processes of photosynthesis, autotrophic and heterotrophic respiration, phenology, turnover, mortality and allocation. This study focuses on assessing the impact of interactive vegetation phenology, i.e. CTEM, on the CRCM5 simulated climate over North America. This is achieved by comparing two CRCM5 simulations—one with interactive phenology and the other with prescribed vegetation, driven by ECMWF reanalysis data (ERA40 and ERA-Interim) at the lateral boundaries, for the 1971–2010 period. Comparison of simulated vegetation attributes, temperature and precipitation in both simulations to those observed indicates that introduction of interactive phenology improves the performance of CRCM5 in some regions, although it introduces new biases in other regions, which are related to the underestimation of leaf area index (LAI). Interactive phenology enhances biosphere–atmosphere interactions, which are reflected in the higher values of correlation between atmosphere and biosphere variables. Interactive phenology also introduces long-term memory in CRCM5, estimated via lagged correlations between precipitation/temperature and LAI. Improved biosphere–atmosphere interactions and long-term memory in the CRCM5 simulation with interactive phenology leads to better interannual variability, particularly noticeable in the biosphere and atmosphere states during anomalously wet and dry years. This study thus provides useful insights related to the added value of interactive phenology in CRCM5 as well as the nature and variability of biosphere–atmosphere interactions over North America.

Keywords Dynamic vegetation model · Interactive phenology · Regional modelling · Biosphere–atmosphere interactions

C. Garnaud (✉) · L. Sushama · D. Verseghy
Département des Sciences de la Terre et de l'Atmosphère, Centre ESCER, Université du Québec à Montréal, Succ. Centre-ville, C.P. 8888, Montreal, QC H3C 3P8, Canada
e-mail: camille.garnaud@gmail.com; camille@sca.uqam.ca

D. Verseghy
Climate Processes Section, Environment Canada, Toronto, Canada

1 Introduction

It is well recognized that climate has a strong influence on the distribution and characteristics of terrestrial ecosystems (Woodward 1987; Stephenson 1990; Prentice et al. 1992; Zhao et al. 2011). In turn, vegetation forcings on climate, through surface characteristics such as albedo and roughness length, have been proven to be important by previous studies based on observations (Liu et al. 2006; Notaro et al. 2006; Wang et al. 2014) and by climate model simulations using static vegetation, i.e. vegetation with prescribed characteristics (Snyder et al. 2004; Dubreuil et al. 2012). However, the study of vegetation impacts on climate using climate models with static vegetation is limited by the fact that these models cannot be expected to adequately capture long-term evolution of vegetation attributes and variability, particularly in the context of changing climate. Pielke et al. (1998) suggest that terrestrial ecosystems could significantly influence atmospheric processes on short-term

(biophysical pathway) as well as on long-term (biogeochemical and biogeographical pathways) timescales, confirming the important role of the biosphere in climate simulations.

Dynamic vegetation models (DVMs) are increasingly being used for applications in climate models to improve the representation of biosphere–atmosphere interactions (Peng 2000; Cox 2001; Quillet et al. 2010; Van den Hoof et al. 2011). A DVM takes into account different terrestrial carbon pools (stems, roots, leaves) and the changes in the terrestrial ecosystem, like vegetation structure and composition, which affect these pools. In these models, vegetation is represented as patches of plant functional types (PFTs) such as crops, grass, deciduous trees, and evergreen trees, with prognostic properties: leaf area index, stem area index, vegetation height, rooting depth, etc. The vegetation attributes change in response to changes in climate in a DVM. These changes include those affecting the biogeochemical, biogeophysical and hydrological cycles, and more specifically alterations in the biomass, productivity and energy fluxes. Consequently, climate models with DVMs are able to simulate vegetation-atmosphere interactions more realistically, particularly in the long term.

Wramneby et al. (2010) studied vegetation-climate feedbacks over Europe under future greenhouse warming using the Rossby Center's Regional Climate Model (RCM) RCA-GUESS, which includes the dynamic vegetation model LPJ-GUESS (Smith et al. 2001), based on two simulations with and without feedbacks of vegetation dynamics. They found that vegetation feedbacks on the climate are small compared to the radiative forcing of increased global CO_2 concentrations but may alter warming projections locally, regionally and seasonally compared to the simulation lacking a dynamic vegetation module. Similarly, using the University of Wisconsin's fully coupled global atmosphere–ocean–land Fast Ocean Atmosphere Model (FOAM) with dynamic vegetation model LPJ, Notaro et al. (2007) showed that, although the majority of the projected future warming is associated with the radiative forcing of rising CO_2, the vegetation physiological forcing augments the warming by weakening the hydrological cycle due to reduced evapotranspiration, particularly for tropical forests. Using the Hadley Center's HadCM3LC with the DVM TRIFFID, Pinto et al. (2009) demonstrated that the lifting condensation level over the Amazon in future conditions could be 1,000 m higher compared to current climate due to reduced vegetation cover, and therefore decreased evapotranspiration leading to low atmospheric humidity resulting in increased sensible heat flux and therefore warmer temperatures.

Several other studies have looked at the effect of vegetation dynamics on the climate variability. Hughes et al. (2006), using the Hadley Center GCM including TRIFFID, found that the variability of the vegetation structure, which is determined by environmental conditions through photosynthesis, and feedbacks can dampen or amplify atmospheric variability through a shift in the response timescale. Delire et al. (2011) using two coupled atmosphere-vegetation models, CCM3-IBIS from the National Center for Atmospheric Research and LMDz-ORCHIDEE from the Institut Pierre Simon Laplace, demonstrated that vegetation dynamics introduces a long-term memory into the climate system by slowly modifying the physical characteristics of the vegetated surface. Furthermore, they found that phenology alone could enhance the variability of the climate system.

Similarly to most of the existing state-of-the-art climate models, including RCMs (Stéfanon et al. 2012; Adam et al. 2014; Kraucunas et al. 2014), the fifth generation of the Canadian RCM (CRCM5) (Zadra et al. 2008; Martynov et al. 2013) is evolving to include a dynamic vegetation module. The land surface scheme used in CRCM5 is the latest version of the Canadian LAnd Surface Scheme (CLASS, version 3.5) (Verseghy 1991, 2011; Verseghy et al. 1993). CLASS recognizes four vegetation types: broadleaf, needleleaf, crops and grass. Vegetation phenology is prescribed in CLASS. The dynamic vegetation model CTEM (Canadian Terrestrial Ecosystem Model: Arora 2003; Arora and Boer 2003, 2005), developed at the Canadian Centre for Climate Modelling and Analysis (CCCma), has been implemented in CRCM5. In this framework, CTEM simulates the vegetation biomass as a function of climate, which is used by CLASS to compute water and energy fluxes at the land–atmosphere interface, allowing a two-way interaction between vegetation and regional climate. The CLASS/CTEM framework has been used in offline simulations and validated against site-specific biophysical and biogeochemical measurements from flux towers (Li and Arora 2011), as well as over all of North America, as detailed in Garnaud et al. (2014). The latter compared two simulations driven by different reanalysis products over North America. They found that the simulated biosphere is relatively sensitive to the driving data, as most simulated carbon pools and fluxes showed important differences, particularly over eastern North America, primarily due to the differences in precipitation and temperature in the driving reanalysis products. Nonetheless, Garnaud et al. (2014) concluded that the simulated biosphere in offline CLASS/CTEM simulations responds adequately to climate change, such as rising CO_2 and temperatures.

The main objective of this study is to assess the impact of interactive vegetation phenology on the CRCM5 simulated climate over North America, particularly the role played by biosphere–atmosphere interactions in modulating the interannual climate variability. This is achieved by comparing two experiments with CRCM5—one with

prescribed vegetation phenology (i.e. CLASS only) and the other with interactive phenology (i.e. CLASS/CTEM), for the 1971–2010 period. The paper is organized as follows. Section 2 gives a brief overview of the model along with a description of the experimental set-up and methods used. Section 3 presents analysis of the RCM simulations, with and without interactive phenology, focusing on the mean state of the simulated climate, biosphere–atmosphere interactions quantified using correlations, long-term memory of the atmosphere and biosphere through lagged correlations, and interannual variability including the state of the biosphere and atmosphere during anomalously dry and wet years. A brief summary and conclusions are given in Sect. 4.

2 Model, experiments and methods

2.1 The Canadian Regional Climate Model

The regional climate model used in this study, CRCM5, is based on a limited-area version of the Global Environment Multiscale (GEM) model used for numerical weather prediction at Environment Canada (Côté et al. 1998). GEM employs semi-Lagrangian transport and (quasi) fully implicit time marching scheme. In its fully elastic nonhydrostatic formulation (Yeh et al. 2002), GEM uses a vertical coordinate based on hydrostatic pressure (Laprise 1992). The following GEM parameterizations are used in CRCM5: deep convection following Kain and Fritsch (1990), shallow convection based on a transient version of the Kuo (1965) scheme (Bélair et al. 2005), large-scale condensation (Sundqvist et al. 1989), correlated-K solar and terrestrial radiation (Li and Barker 2005), subgrid-scale orographic gravity-wave drag (McFarlane 1987), low-level orographic blocking (Zadra et al. 2003), and turbulent kinetic energy closure in the planetary boundary layer and vertical diffusion (Benoit et al. 1989; Delage and Girard 1992; Delage 1997).

The land surface scheme CLASS in CRCM5 models three soil layers, 0.1, 0.25 and 3.75 m thick in its standard formulation, corresponding approximately to the depth influenced by the diurnal cycle, the rooting zone and the annual variations of temperature, respectively. CLASS includes prognostic equations for energy and water conservation for the three soil layers and a thermally and hydrologically distinct snowpack where applicable (treated as a fourth variable-depth layer). The thermal budget is performed over the three soil layers, but the hydrological budget is done only for layers above the bedrock. In order to simply mimic subgrid-scale variability, CLASS adopts a "pseudo-mosaic" approach and divides the land fraction of each grid cell into a maximum of four sub-areas: bare soil, vegetation, snow over bare soil and snow with vegetation. The energy and water budget equations are first solved for each sub-area separately and then averaged over the grid cell, using spatially varying structural attributes and physiological properties of the four CLASS PFTs in CLASS (needleleaf trees, broadleaf trees, crops and grasses). These structural attributes include albedo, leaf area index (LAI), roughness length, canopy mass and rooting depth.

The dynamic vegetation model CTEM that has recently been implemented in CRCM5 is a process-based ecosystem model (Arora 2003; Arora and Boer 2003, 2005, 2006; Li and Arora 2011) designed to simulate the terrestrial carbon cycle. It is able to grow vegetation from bare ground and to simulate several vegetation structural attributes such as leaf area index, vegetation height, root distribution and canopy mass. It includes processes such as photosynthesis, autotrophic respiration, heterotrophic respiration, phenology, turnover, allocation, fire and land-use change. CTEM simulates two dead carbon pools—litter and soil organic carbon—and three live vegetation pools—stems, leaves and roots. Terrestrial ecosystem processes in CTEM are modeled for nine different plant functional types (PFTs): evergreen and deciduous needleleaf trees, broadleaf evergreen and cold and drought deciduous trees, and C_3 and C_4 crops and grasses. The manner in which CLASS and CTEM interact is explained in the following section.

2.2 Experiments

As discussed earlier, this study investigates the effects of interactive phenology on the regional climate and its variability over North America. Two simulations are performed for the 1958–2010 period at 0.5° resolution; these simulations are forced by the European Center for Medium range Weather Forecast's (ECMWF) ERA40 reanalysis data (Uppala et al. 2005) for the 1958–1978 period and by ERA-Interim reanalysis data (Dee et al. 2011) for the 1979–2010 period at the lateral boundaries. The ERA40 reanalysis (Uppala et al. 2005) is available for the period 1957–2001 at 2.5° (~250 km) resolution. The ERA-Interim reanalysis (Dee et al. 2011) is available from 1979 to the present day at a resolution of 1.5°.

The first simulation uses prescribed vegetation phenology (i.e. standard vegetation phenology used currently in CRCM5) and the second uses interactive vegetation phenology (i.e. CTEM; Fig. 1). These two simulations will be referred to hereafter as CRCM5_STD and CRCM5_CTEM, respectively. The two simulations are run at a 20-min time step and are forced with observed CO_2 concentrations from the NASA Earth Sciences Division (Hansen and Sato 2001, 2004). Thus, the carbon cycle feedbacks are not included. The soil type, i.e. percentage of sand and clay, for the three layers modeled in CLASS is taken from Webb et al. (1991).

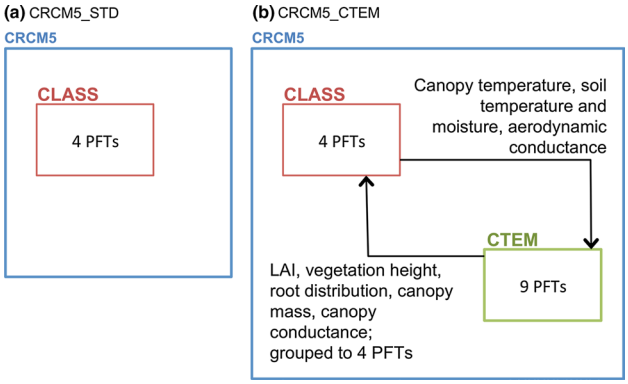

Fig. 1 Schematic diagram demonstrating the representation of vegetation PFTs in (**a**) CRCM5_STD and (**b**) CRCM5_CTEM simulations. The interactions between CTEM and CLASS are also shown in CRCM5_CTEM. *PFT* Plant Functional Type, and *LAI* leaf area index

The grid cell fractional coverage of nine PFTs, shown in Fig. 2, is obtained from the HYDE 2 database (Klein Goldewijk 2001; Arora and Boer 2010) for crops and from Wang et al. (2006) for other PFTs. The land fractional cover is specified at its 1960 values. It should be noted that in CRCM5_CTEM, even though the geographical distribution of PFTs is fixed, the vegetation attributes (LAI and carbon pools) are simulated as dynamic functions of driving climate. The sea surface temperatures (SST) and sea ice concentrations (SIC) in the CRCM5 simulations are prescribed from AMIP2 (Atmospheric Model Intercomparison Project; Taylor et al. 2000) for the 1958–1978 period and from ERA-Interim (Dee et al. 2011) for the 1979–2010 period. No spectral nudging was used. Consequently, the differences in simulated climate between CRCM5_STD and CRCM5_CTEM are due only to the differences in interactions between the vegetation and the atmosphere. Initial conditions of soil and vegetation state were obtained by running CLASS/CTEM offline for 300 years driven by repeated temperature, humidity and wind variables from a 20-year CRCM5 simulation (with CTEM, and initialized using data from Garnaud et al. 2014), until equilibrium conditions were obtained, using a fixed 1765 CO_2 concentration during the first 107 years and a transient 1765–1957 CO_2 concentration for the following 193 years. The vegetation parameters prescribed in CRCM5_STD (albedo, max and min LAI, rooting depth, etc.) are derived from the biosphere state during the last 50 years of the above-mentioned 300-year offline simulation.

2.2.1 CRCM5_STD versus CRCM5_CTEM

The most important differences between CRCM5_STD and CRCM5_CTEM, i.e. simulations with prescribed and interactive vegetation phenology respectively, relate to the canopy resistance and photosynthesis, phenology, root distribution, canopy mass and vegetation height.

Photosynthesis and canopy conductance are of crucial importance in vegetation modelling. In CRCM5_STD, the canopy conductance ($g_c = 1/r_c$) formulation handled in CLASS is similar to that of Schulze et al. (1995), where the canopy resistance (r_c) is expressed as a function of minimum stomatal resistance (r_{min}) and a series of environmental dependences, such as incoming solar radiation, air temperature, vapour pressure deficit and soil moisture suction. Thus, the effect of atmospheric CO_2 concentration on canopy resistance is not explicitly modeled in this formulation.

In CRCM5_CTEM, CTEM models photosynthesis, as described in detail in Arora (2003). In addition to the environmental variables cited above, the CTEM formulation includes the effect of atmospheric CO_2 concentration on stomatal conductance. This is essential to simulate the physiological effects of increasing CO_2 amounts on stomatal conductance, and thus canopy resistance, in climate simulations. The photosynthesis sub-module used in CTEM is based on the biochemical approach (Farquhar et al. 1980; Collatz et al. 1991, 1992) with some minor differences. The photosynthesis rate, A, is co-limited by assimilation rates based on the photosynthetic enzyme Rubisco, the amount of available light, and the photosynthetic product transport capacity. CTEM can also simulate the effect of soil moisture stress on photosynthesis in order to account for soil moisture stress via stomatal closure. Net canopy photosynthesis rate, A_n, is then used to estimate canopy conductance. A_n is obtained by subtracting canopy leaf maintenance respiration from the canopy photosynthesis rate (Arora 2003). Thus, when CTEM is coupled to CRCM5/CLASS, the canopy conductance is estimated by CTEM's photosynthesis sub-module, which uses canopy temperature, aerodynamic conductance, soil moisture and other variables simulated by CLASS. CLASS and CTEM's photosynthesis sub-module, simulating the fast biophysical processes, such as photosynthesis, canopy conductance and leaf respiration, operate at the model timestep (20 min) while other biogeochemical processes are modeled at a daily timestep. The canopy conductance is then passed back to CLASS, where it is used in its energy and water balance calculations.

With respect to phenology, in CRCM5_STD, CLASS adopts an approach where the air temperature and the temperature of the top soil layer determine leaf onset and offset, as described in Verseghy (2011). A threshold air temperature of 2 °C is used and when this threshold is exceeded the LAI increases linearly from a specified minimum to specified maximum value in certain number of days: 2 months for needleleaf trees and 1 month for broadleaf trees. With respect to crops, the Earth is divided into 10° latitude bands, and as specified in Verseghy (2011), the

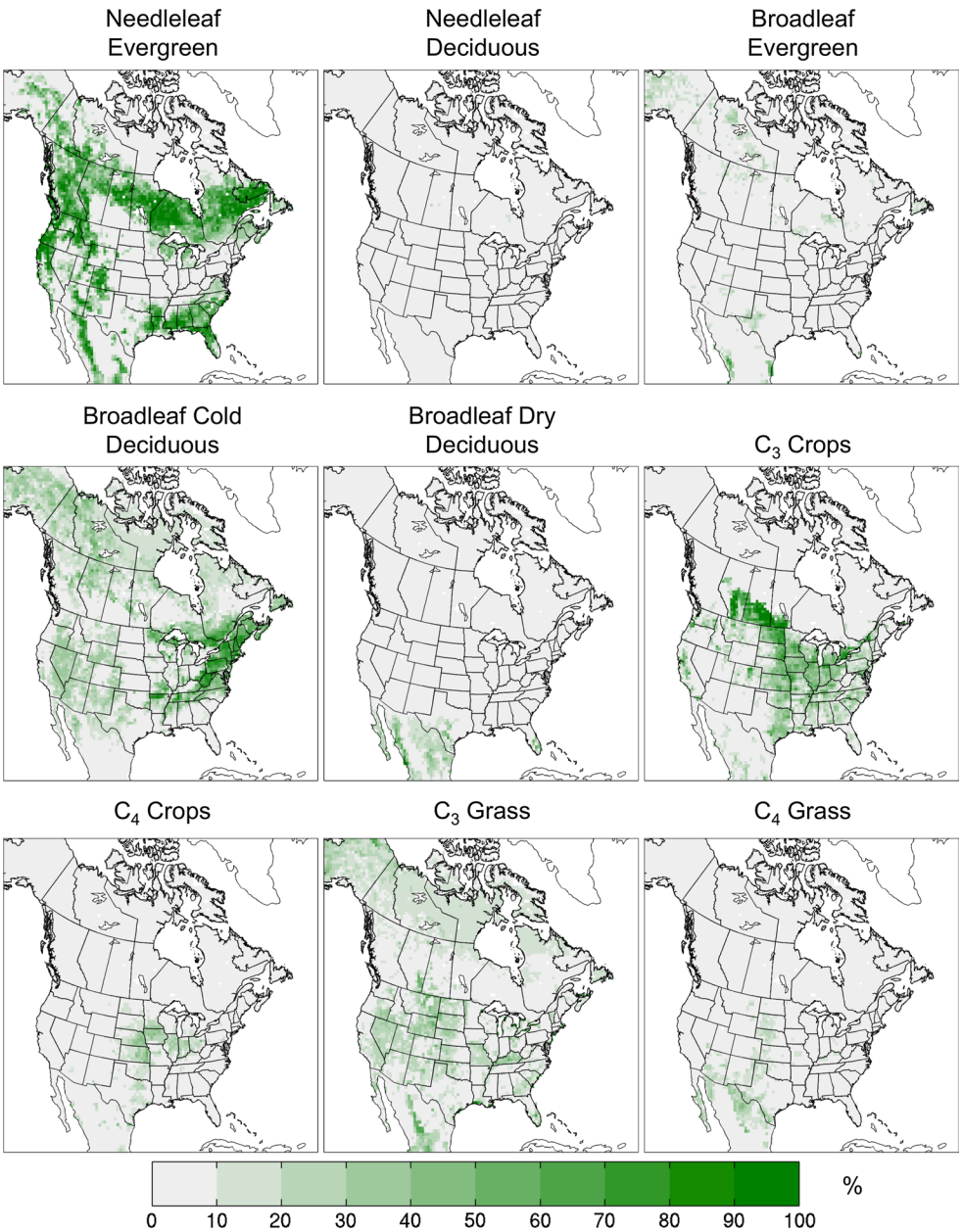

Fig. 2 Fractional coverage (%) of the nine Plant Functional Types (PFT) considered in CTEM for the North American study domain

beginning of crop growth and the end of harvest are specified for each band as occurring on certain days of the year. It is assumed that crops take 2 months to reach maturity, and that 1 month elapses between the time that senescence begins and the time that harvest is over. Since the annual variations in height and leaf area index of grass can be considered as negligible, its height and LAI are assigned to a maximum value throughout the year. Thus, seasonality is modeled but not long-term variations in canopy cover or vegetation structure.

In CRCM5_CTEM, CTEM simulates the leaf onset through a carbon benefit approach, and the leaf offset is initiated by unfavorable environmental conditions that stress the plant and imply carbon loss. These unfavorable conditions include shorter day length, cooler temperatures, and drier soil moisture conditions. These processes are fully described in Arora and Boer (2005). In CTEM, four plant growth states determine the plant behavior and allocation patterns, as summarized in Table 2 of Arora and Boer (2005). These are maximum growth, normal growth, leaf-fall/crop-harvest and dormancy/no-leaves. During maximum growth, for trees and crops, all net primary productivity is allocated to leaves. For grass, the allocation is to leaves and roots for structural stability reasons. During normal growth, the allocation is shared between leaves, stem (if applicable) and roots. During leaf fall and crop harvest, the allocation to leaves ceases but continues for stem and roots. During dormancy/no-leaf state, no allocation occurs

in the absence of CO_2 uptake. The set of conditions used to trigger transition from one plant state to another for each PFT in CTEM are described in Arora and Boer (2005).

In CRCM5_STD, CLASS calculates the vegetation height and the canopy mass as a function of a PFT-dependent roughness length for momentum at vegetation maturity and maximum value of canopy mass, respectively. For trees, these values are invariant; for crops and grass, the vegetation effective height and the canopy mass vary annually with snow depth and growth stage. The rooting depth remains at its PFT-dependent maximum value for trees and grass; for crops, it is further corrected for growth stage.

In CRCM5_CTEM, CTEM allocates positive net primary production (NPP) between leaf, stem, and root components, which increases their biomass, while negative NPP results in the decrease of component biomass because of respiration. As a result of these allocation processes, the vegetation biomass may vary diurnally. CTEM then uses the simulated leaf biomass to calculate the LAI, which is passed on to CLASS and used in energy and water balance calculations over the vegetated fraction of the grid cell. The root biomass is converted to a rooting depth and root distribution profile through a variable root distribution parameterization (Arora and Boer 2005), and they are then used to estimate the fraction of roots in each soil layer required for calculating transpiration in CLASS. The aboveground canopy mass from CTEM is used to estimate the canopy heat capacity.

In CRCM5_CTEM, the vegetation structural attributes of CTEM's nine PFTs are clustered to four PFTs (needleleaf trees, broadleaf trees, crops and grass) when they are passed on to CLASS (see Fig. 1). CLASS and CTEM's photosynthesis sub-module that simulates the fast biophysical processes, such as photosynthesis, canopy conductance and leaf respiration, operates at a 20 min timestep while the rest of CTEM runs at a daily timestep.

2.3 Methods of model output evaluation and analysis

Prior to studying the impact of interactive phenology on the simulated climate over North America, the climate and biosphere simulated by CRCM5_STD are compared to observations in order to assess the model performance and to help identify biases. CRCM5_STD simulated temperature and precipitation are compared to gridded observational datasets available from the Climate Research Unit (CRU) (Mitchell and Jones 2005) and from the University of Delaware (UDEL) (Willmott and Matsuura 1995). The CRU TS 2.1 dataset covers the period 1901–2002 at a monthly temporal resolution and has a spatial resolution of 0.5°. The UDEL V3.01 dataset is composed of monthly values from 1901 to 2010 with a 0.5° global coverage. The simulated biosphere is evaluated against the observation-based green leaf area index product from the International Land Surface Climatology Project Initiative (ISLSCP II) FASIR-adjusted NDVI Biophysical Parameter Fields measured by the satellite mounted AVHRR sensor (Los et al. 2000; Hall et al. 2006; Sietse 2010). This monthly global dataset is available for the 1982–1998 period at 0.5° × 0.5° resolution. To limit the impact of initial conditions on results, the analysis presented in this study focuses on the 1971–2010 period. The impact of interactive vegetation phenology on the simulated climate over North America is then investigated by comparing CRCM5_CTEM and CRCM5_STD, particularly with respect to biosphere–atmosphere interactions.

To assess the strength of the simulated biosphere–atmosphere interactions, statistical analyses are performed. First Pearson correlation coefficients are computed to determine the strength of the linear relationships between maximum leaf area index, precipitation, temperature, and sensible and latent heat fluxes (SHF and LHF) during spring and summer seasons. Where required, this is followed by a path analysis (Pinto et al. 2009) to decompose the Pearson correlations into direct (β_i) and indirect (β_j) effects of two independent variables (x_i and x_j) on a dependent variable (y), using the relation:

$$r_i = \beta_i + \beta_j c(x_i, x_j), \quad \text{for } i = 1, 2 \text{ and } i \neq j, \tag{1}$$

where r_i is the Pearson correlation coefficient between x_i and y, β_i is the standardized coefficient of x_i estimated from multiple linear regression and $c(x_i, x_j)$ is the correlation coefficient between x_i and x_j. The indirect effect can be seen as the effect of x_j on y resulting from interaction with x_i.

Any long-term memory introduced by interactive phenology is studied through lag correlations. Also, the interannual variability of selected biosphere and climate characteristics in both simulations is investigated using the coefficient of variation (i.e. the ratio of the standard deviation to mean). In connection with the interannual variability, modeled atmosphere and biosphere states for observed anomalously dry/hot and wet years are also studied. To this end, the year 1988, which was a very dry and warm year over large regions of the United States, covering the central and eastern parts, is selected. The year 1993, which was an anomalously wet year over approximately the same region, is also considered. For the dry and warm year of 1988, the simulated number of hot days (NHD) is compared to that observed. Using a similar approach to Fischer et al. (2007), NHD is defined as the number of days with maximum temperature exceeding the long-term (1981–2010) 90th percentile daily maximum temperatures, calculated for each month of the summer (JJA) season. Since no single high-resolution dataset of daily temperature is available over the study domain, two observation datasets, covering Canada and the USA, were used. The gridded observational dataset over Canada (Hopkinson et al. 2011) is generated from

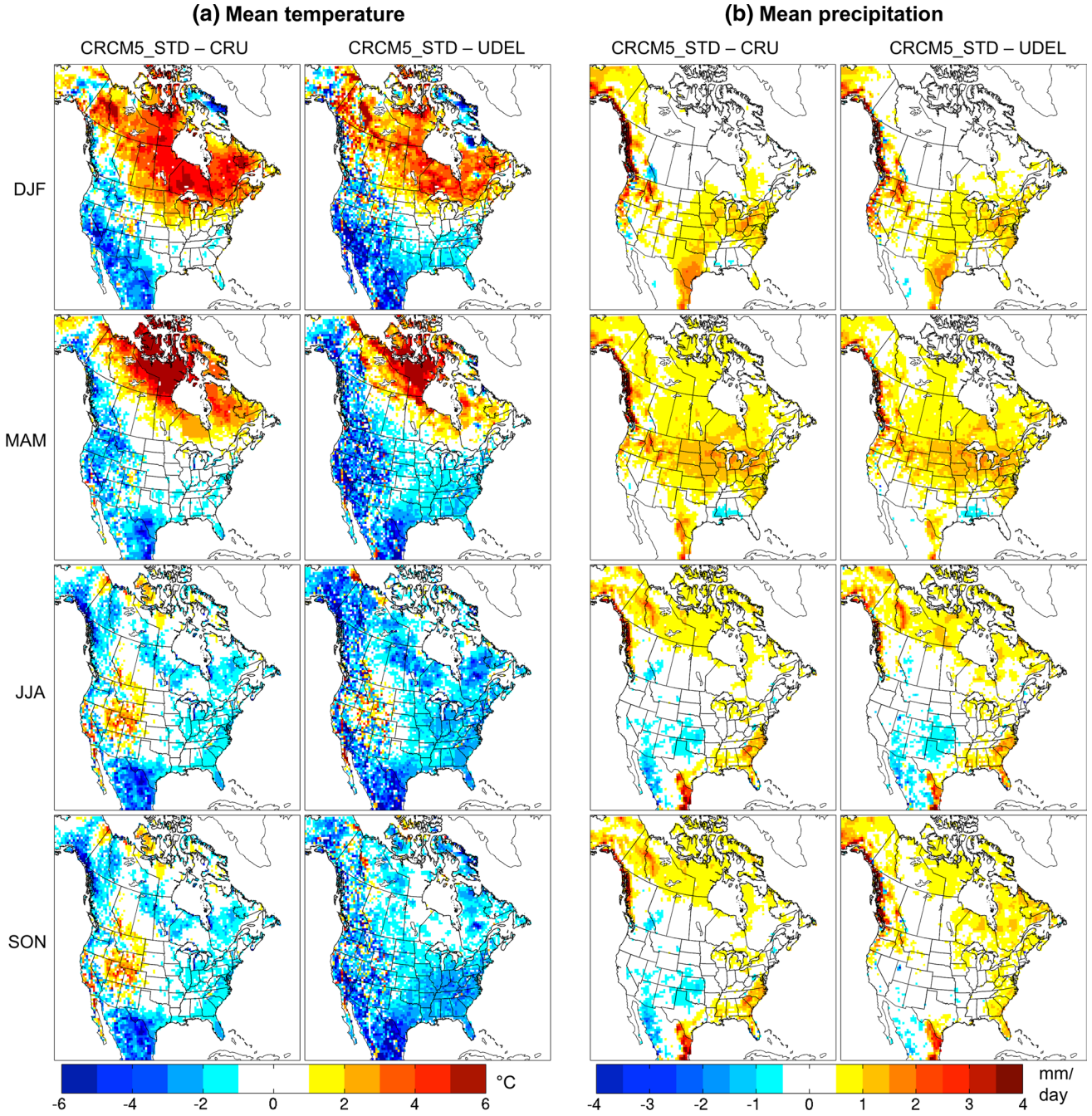

Fig. 3 Differences in mean seasonal (**a**) temperature (°C) and (**b**) precipitation (mm/day) between CRCM5_STD and CRU (columns 1 and 3) and between CRCM5_STD and UDEL (columns 2 and 4) for the 1971–2010 period

daily observations at Environment Canada climate stations using a thin plate smoothing spline surface fitting method. The gridded meteorological data from the University of Washington (UW; Maurer et al. 2002) is used over the USA. The response of the biosphere in CRCM5_STD and CRCM5_CTEM to the anomalous amounts of precipitation and temperatures for the studied dry and wet years is also explored in detail.

3 Results and discussion

3.1 CRCM5_STD evaluation

The mean seasonal temperature and precipitation modeled by CRCM5_STD for the 1971–2010 period are compared with those from the CRU and UDEL datasets in Fig. 3. It should be noted that there are large differences between

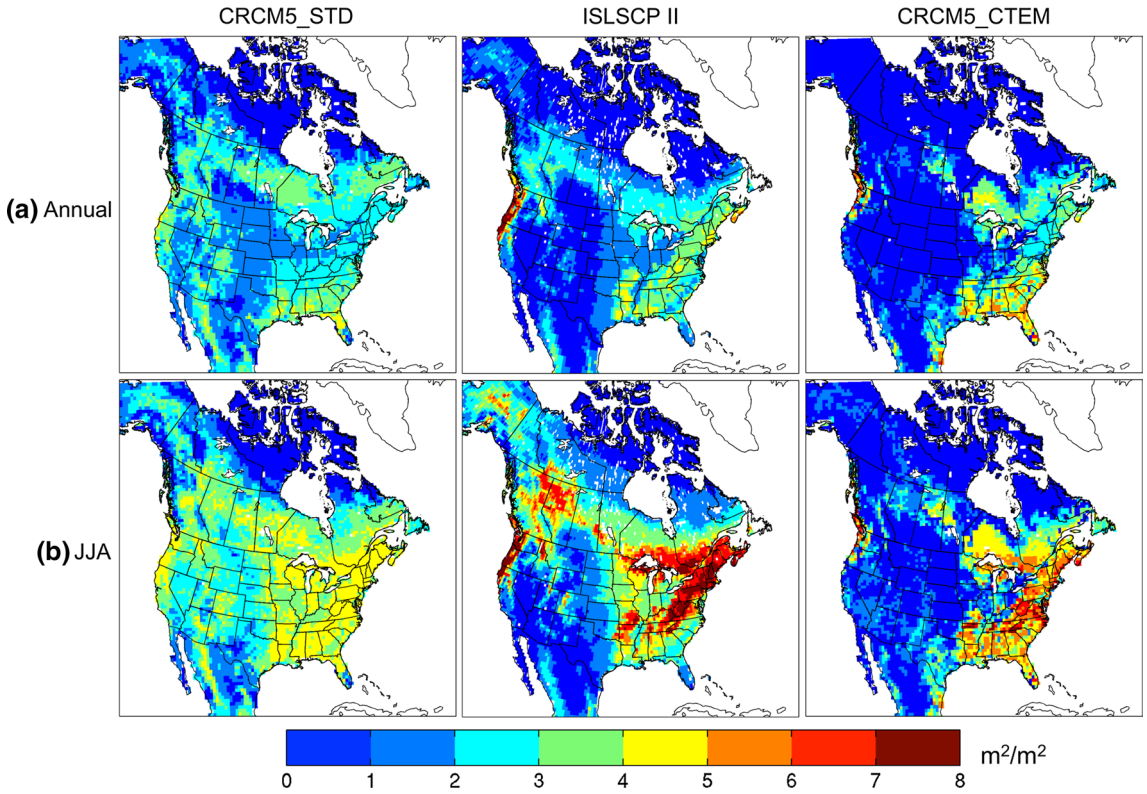

Fig. 4 Spatial plots of the mean (**a**) annual and (**b**) summer LAI (m^2/m^2) (1982–1998) for CRCM5_STD (1st column), CRCM5_CTEM (3rd column) and the ISLSCPII data (2nd column) from Los et al. (2000), Hall et al. (2006) and Sietse (2010)

CRU and UDEL datasets, especially in the northern high latitudes where observations are scarce. However, deviations in the simulated climate are generally larger than differences between the two datasets (CRU and UDel). In winter (DJF) and spring (MAM), there is a warm bias over Canada, which is more pronounced when compared to the CRU data. From Mexico to western US, a cold bias persists most of the year. The comparison with the UDEL dataset also shows a cold bias along the east coast of the US that is more widespread during summer (JJA) and autumn (SON). With respect to precipitation, CRCM5_STD generally overestimates. There is a wet bias over the Canadian west coast that is strongest in winter and autumn, and weakest in summer. A wet bias is also noticeable over large parts of central and eastern US in winter, and it extends over Canada in spring. Since CRCM5_STD is driven by ERA-40/ERA-Interim, these biases, generally referred to as performance errors, are related to the internal dynamics and physics of the model.

The mean annual and summer values of LAI from CRCM5_STD are compared to the ISLSCP II data for the 1982–1998 period in Fig. 4. With respect to the annual mean LAI, though the general spatial pattern is reasonably well captured, CRCM5_STD tends to overestimate the LAI over central and western US, and over north-eastern Canada, where most of the vegetation consists of crops and/or grass in the model. LAI is underestimated along the central west coast. Since the annual LAI is an average of all seasons, Fig. 4b focuses more specifically on the summer season, where the overestimation over central and western US is more pronounced. There is also a strong underestimation of LAI over eastern US and southeastern-most Canada, which are mainly covered by broadleaf trees. Underestimation of LAI along the central west coast is still present. These PFT-specific biases are probably due to the formulation of the vegetation attributes in CLASS, particularly the LAI. Furthermore, it is not possible to make direct linkages with precipitation and temperature, as interannual variations in climate do not affect the prescribed vegetation attributes in CRCM5_STD.

3.2 Mean climate: CRCM5_STD versus CRCM5_CTEM

Both CRCM5_STD and CRCM5_CTEM simulations have the same grid cell fractional vegetation coverage (Fig. 2). However, the vegetation state and its evolution are different in the two simulations, as discussed in Sect. 2.2. This results in dissimilarities in the simulated LAI. When looking at the annual mean LAI simulated by CRCM5_CTEM (Fig. 4), there is an overall improvement over eastern North

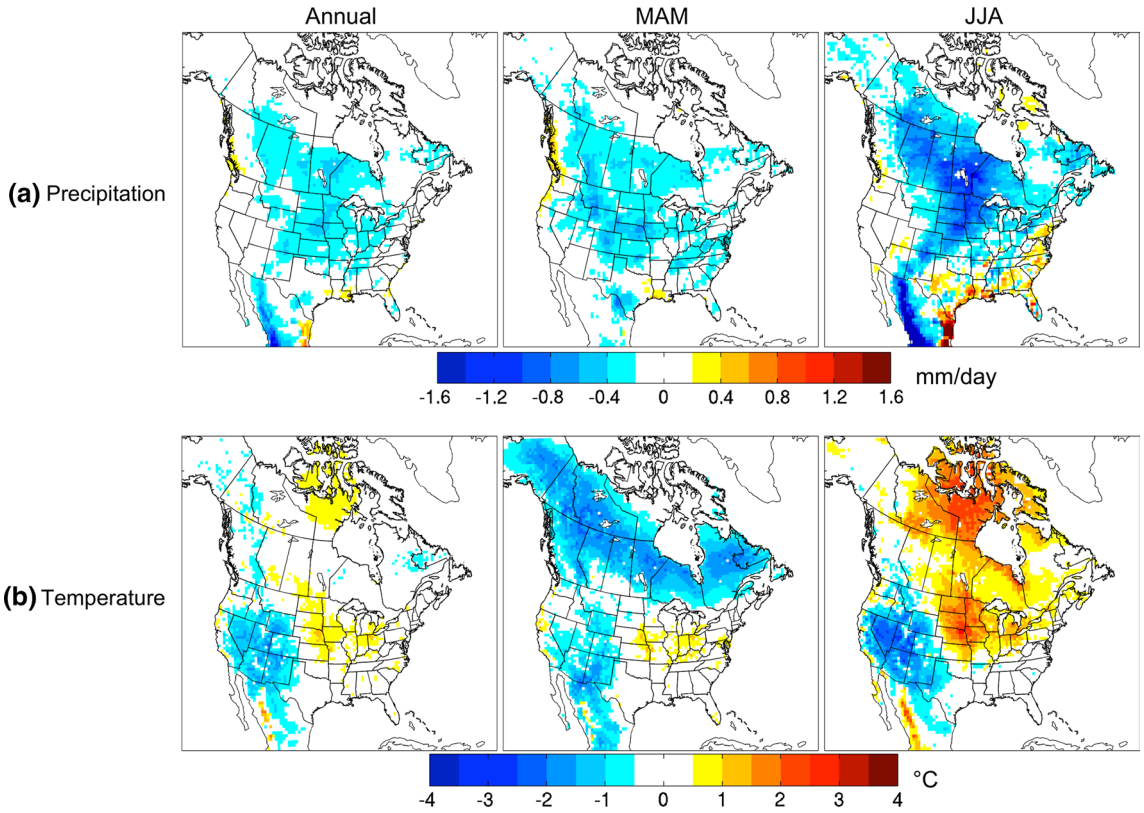

Fig. 5 Differences in the annual (1st column), spring (MAM; 2nd column) and summer (JJA; 3rd column) mean (a) precipitation (mm/day) and b) temperatures (°C) between CRCM5_CTEM and CRCM5_STD for the 1971–2010 period

America compared to CRCM5_STD, but not over western Canada, where the boreal forest is underestimated by CRCM5_CTEM. However, the LAI along the central west coast is much improved, which could come from a LAI-precipitation positive feedback since CRCM5_CTEM has more precipitation than CRCM5_STD in this area, as seen in Fig. 5a. There is a slight overestimation of LAI over southeast US in CRCM5_CTEM. More specifically, during summer, CRCM5_CTEM does a better job compared to CRCM5_STD at portraying the LAI over eastern North America, although it is still underestimated.

The underestimation of LAI in CRCM5_CTEM over the western boreal forest is clearly visible for summer. This could be due to a negative LAI-temperature feedback in spring. Comparison of CRCM5_CTEM and CRCM5_STD in Fig. 5b shows that CRCM5_CTEM simulates much cooler temperatures in spring over the boreal region, which may lead to a lower annual and summer LAI by delaying the annual increase in LAI of evergreen needleleaf trees. It is worth noting that, in Garnaud et al. (2014), ERA40- and NCEP-driven CLASS/CTEM offline simulations showed a similar underestimation of LAI in the western boreal forest. Also, results from Peng et al. (2014) show that, while the needleleaf evergreen PFT of the model performs well for the coast of British Columbia, it yields lower than observed GPP in the interior of the province. This is due to the colder and drier climate in the interior of British Columbia, to which CTEM's needleleaf evergreen trees are not adapted. These results indicate that while the broad classification of PFTs in CTEM is sufficient to capture terrestrial ecosystem process at the global scale, it is inadequate for representing regional scale processes and another needleleaf evergreen PFT is probably required, as suggested by Peng et al. (2014). However, it must be noted that there are large uncertainties in the observation datasets. For example, Gibelin et al. (2006) showed that the ISLSCP II LAI is higher than other satellite based estimates, especially for the boreal forest. Garrigues et al. (2008) also showed that LAI datasets derived from remote sensing data all have their weaknesses, especially over forests. The underestimation of LAI over central and eastern North America is mainly due to the weak representation of C_3 crops in CTEM, and this bias was also reported in Garnaud et al. (2014), but it is probably amplified by the lower precipitation in CRCM5_CTEM over central North America (Fig. 5a). On the contrary, the LAI of crops is overestimated in CRCM5_STD compared to observations, thus creating large differences between the two simulations.

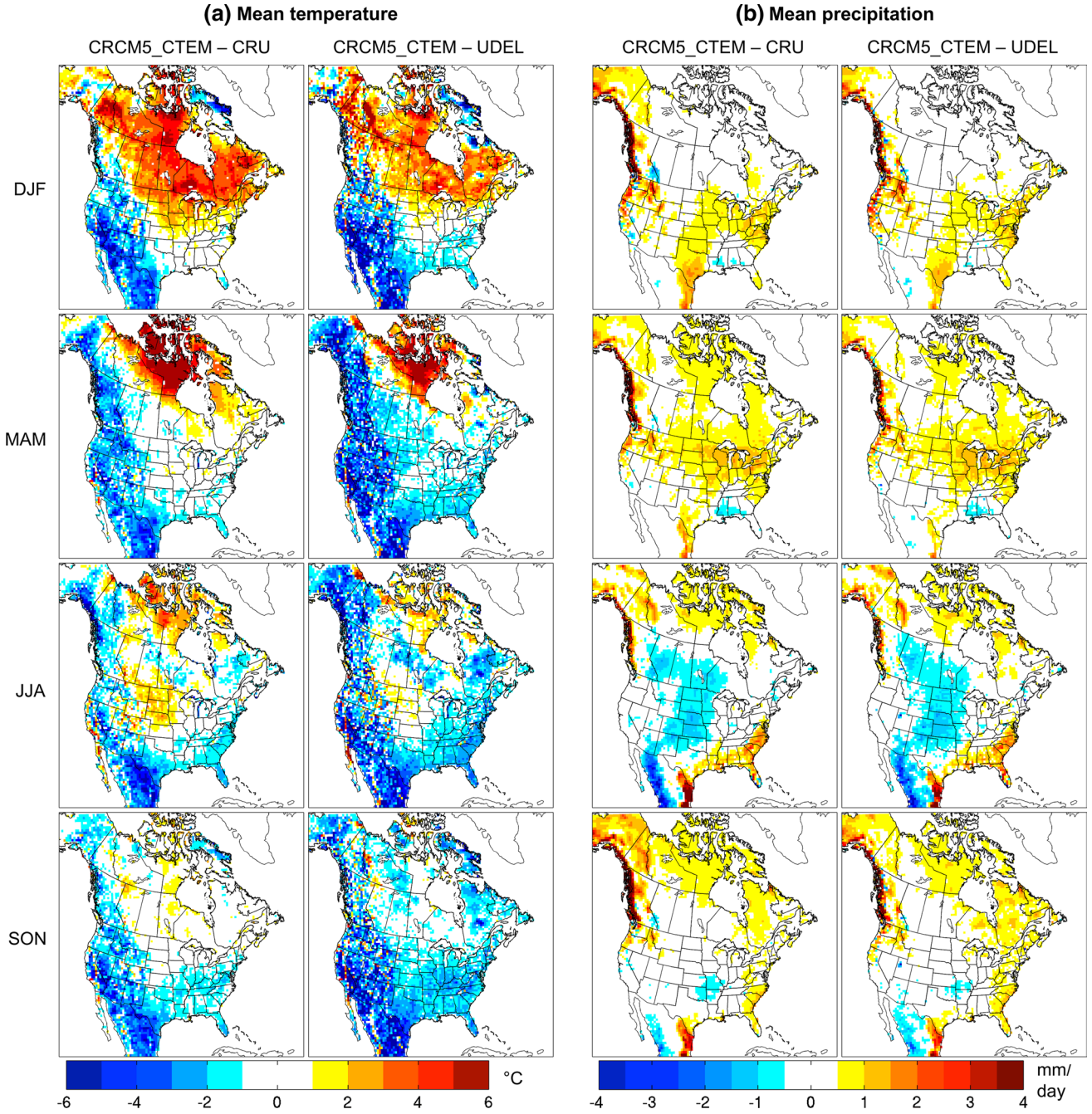

Fig. 6 Differences in mean seasonal (**a**) temperature (°C) and (**b**) precipitation (mm/day) between CRCM5_CTEM and CRU (columns 1 and 3) and between CRCM5_STD and UDEL (columns 2 and 4) for the 1971–2010 period

The LAI is the vegetation characteristic that has the largest impact on the biosphere–atmosphere interactions, and is thus the best characteristic to describe the state of the biosphere with respect to surface energy and water fluxes (Delire et al. 2004). Therefore, one could assume that the large differences in the LAI between CRCM5_STD and CRCM5_CTEM would lead to differences in climate, especially during the growing season. Figure 6 shows the differences in the mean temperature and precipitation (columns a and b, respectively) between CRCM5_CTEM and the CRU and UDEL datasets during the 1971–2010 period. As shown in Fig. 5b, the largest differences between CRCM5_CTEM and CRCM5_STD in temperature occur in spring and summer. A comparison of Fig. 3a with Fig. 6a shows that CRCM5_CTEM tends to decrease the overestimation of the temperature over Canada in CRCM5_STD in

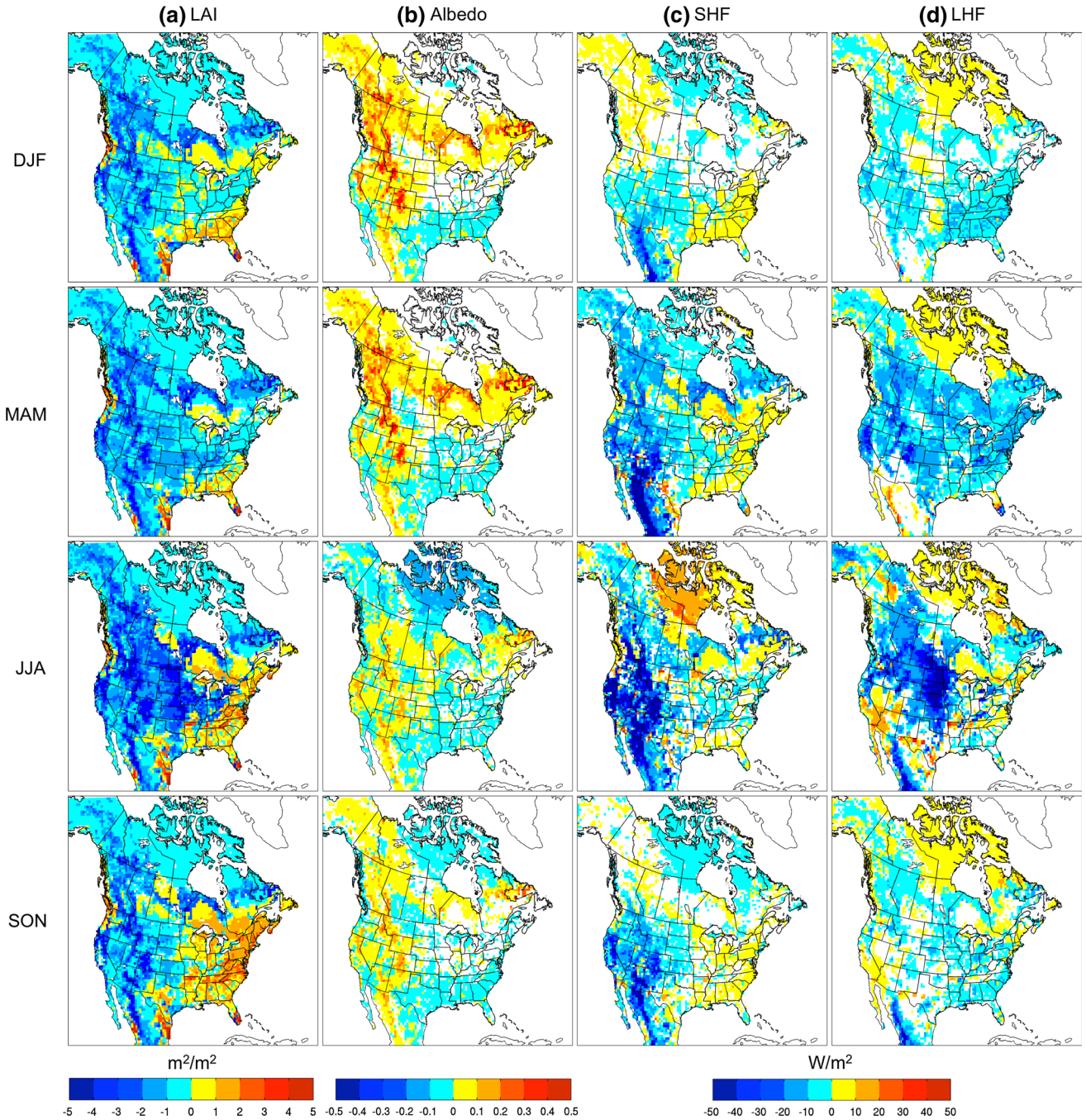

Fig. 7 Seasonal differences in (**a**) LAI (m^2/m^2), (**b**) albedo, and (**c**) sensible and (**d**) latent heat fluxes (W/m^2) between CRCM5_CTEM and CRCM5_STD for the 1971–2010 period. Regions where differences are not statistically significant are shown in *white*; significance is calculated using the Student's *t* test at 5 % significance level

the high latitudes in spring, but increases the cold bias over Mexico and southwest US.

Figure 7 shows the seasonal differences in LAI, albedo, SHF and LHF between CRCM5_CTEM and CRCM5_STD for the 1971–2010 period; values are shown only for grid cells where the differences are statistically significant at 5 % significance level, estimated using Student's *t* test. During spring season in CRCM5_CTEM, for the mid- to high-latitudes, cooler temperatures lead to greater snow depth (figure not shown), partially masking the vegetation (particularly grass) and thus reducing the exposed LAI compared to CRCM5_STD (Fig. 7a), resulting in higher albedo, as shown in Fig. 7b. This leads to further reduction of the temperatures in CRCM5_CTEM

compared to CRCM5_STD (Fig. 5b) through decreased SHF (Fig. 7c). CTEM also reduces the cold bias over Canada in summer in CRCM5_STD (Fig. 3a) due to the lower albedo (Fig. 7b), but in some areas warm biases are introduced in CRCM5_CTEM (Fig. 6a). The albedo effect in the boreal regions is strong in summer and leads to an increased SHF (Fig. 7c) in CRCM5_CTEM, resulting in warmer temperatures (Fig. 3b) compared to CRCM5_STD. Furthermore, CRCM5_CTEM mostly reduces the warm bias over the Rocky Mountains in western US in summer (Fig. 6a) compared to CRCM5_STD because of a significant decrease in SHF (Fig. 7c) due to a decrease in LAI (Fig. 7a) and an increase in albedo (Fig. 7b), which once again leads to cold biases in some areas in CRCM5_CTEM. These arid regions with large fractional areas of bare ground have higher albedo values. Moreover, CRCM5_STD shows a cold bias over Mexico and western US (Fig. 3a) all year long, thus the significantly lower LAI in CRCM5_CTEM (Fig. 7a) in these regions generally increases the temperature bias (Fig. 6a), although CRCM5_CTEM's LAI is closer to the observations (Fig. 4). In this area, a decrease in LAI leads to an increase in albedo and to a cooling of the 2-m temperature.

The effect of the biosphere on precipitation is more complex as the precipitation source could be local recycling or convergence of moisture advected into the region. As shown in Figs. 5a and 6b, similar to the temperatures, the largest differences between the two simulations occur in spring and summer, when the biosphere–atmosphere interactions are strong. CRCM5_CTEM only slightly improves the dry bias along the west coast compared to CRCM5_STD, despite the difference in LAI (Fig. 7a), as the main source of precipitation in this region is the moisture advected into the region. In spring, the lower LAI in CRCM5_CTEM (Fig. 7a) across western and central US implies reduced LHF (Fig. 7d), which could lead to reduced contribution of local moisture to the total atmospheric westerly transport of transpired water. In summer, the differences in LAI are strongest between the two simulations (Fig. 7a). This is the season with maximum convective activity and therefore the biosphere has a more direct effect on the local precipitation. The model is able to reproduce these biosphere–atmosphere interactions: in summer, the spatial patterns of the differences in LHF (Fig. 7d), a variable that is greatly affected by LAI, and precipitation (Fig. 5a) are very similar.

However, the main patterns of biases to CRU and UDel in both temperature and precipitation remain after dynamic coupling of vegetation. This is an indication that the biases could be due to deficiencies in model physics (not related to vegetation) or due to errors in the driving data and model resolution.

Thus, although the impact of interactive phenology on the 1971–2010 mean climate can be significant depending on the region and the season, it does not always improve the model when compared to observations. However, the possible improvement from CTEM is limited by its own internal biases, along with the biases from the simulated climate, greatly influencing the simulated vegetation. Indeed, Garnaud et al. (2014) have shown that the vegetation simulated by CLASS/CTEM is sensitive to the driving climate. Despite these limitations, the implementation of CTEM in CRCM5 enables better representation of certain aspects of biosphere–atmosphere interactions, as discussed in the following section.

3.3 Biosphere–atmosphere interactions: CRCM5_STD versus CRCM5_CTEM

Figure 8 shows spatial plots of the correlations between the annual maximum LAI and the mean spring–summer (MAMJJA) precipitation, LHF, temperature and SHF. In CRCM5_STD, the correlations between maximum LAI and precipitation, LHF and SHF (Fig. 8a, b, d, respectively) are mostly non-significant, which is expected since the links between these variables in the model are weak. However, positive correlations are seen between the LAI and the temperature (Fig. 8c) in the high-latitudes in CRCM5_STD. This is because temperature is the main determining factor of leaf phenology in this simulation. Once the conditions with respect to 2-m air temperatures are favorable (i.e. above 2 °C), LAI increases from a minimum value to a maximum value (both prescribed) in a predefined amount of time. Thus, if the temperatures are too low in a given year, the plants will not have time to reach their maximum LAI, and hence the positive correlations in the high latitudes.

In CRCM5_CTEM, the correlations between the LAI and precipitation are very strong with mainly positive values (Fig. 8a). Over southern North America for example, where water is a growth-limiting factor, vegetation is largely dependent on precipitation. This leads to a positive LAI-precipitation feedback loop, with a positive precipitation anomaly boosting plant productivity and LAI, which leads to increased evapotranspiration, as shown in Fig. 8b, and possibly the amount of local rainfall. In the northern latitudes, the strong positive correlations between LAI and precipitation may be the result of both the increased LHF contributing to local rainfall and the reduced heat stress due to increased cloud cover. The correlations between the LAI and temperature (Fig. 8c) are negative over southern North America, since plants suffer from heat stress at higher temperatures in these regions, consequently decreasing the vegetation productivity. The correlations are positive in the higher latitudes, where vegetation will benefit from warmer

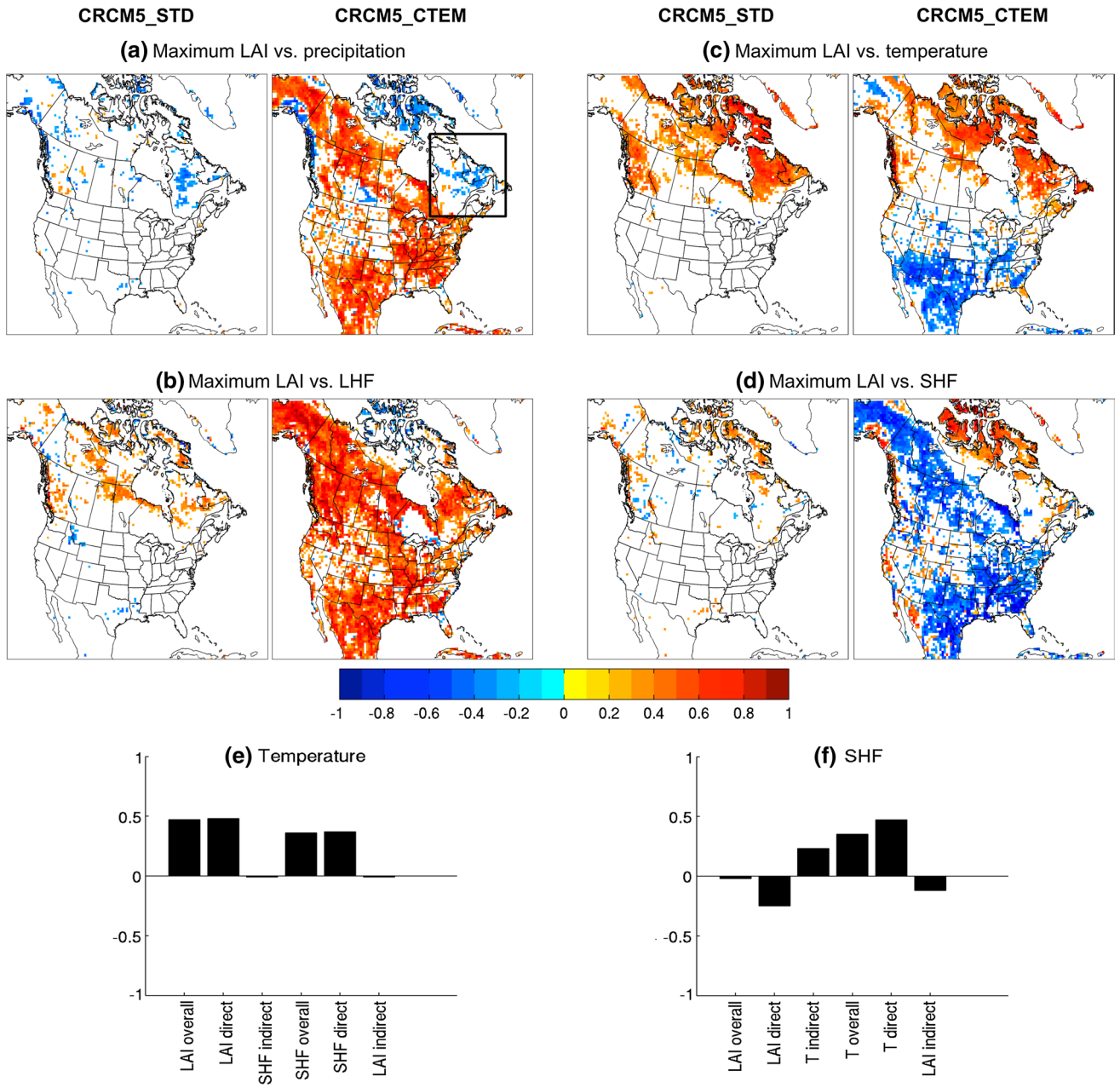

Fig. 8 Spatial plots of the correlations between the maximum LAI and mean spring/summer **a** precipitation, **b** LHF, **c** temperature, and **d** SHF for the 1971–2010 period. Regions where correlations are not significant are shown in *white*; significance is calculated using the Student's *t* test at 10 % significance level. Path analysis illustrating the direct, indirect and overall effects of **e** maximum LAI and SHF on temperature, and **f** maximum LAI and temperature (T) on SHF, in CRCM5_CTEM in the region defined by the *black box* in (**a**)

temperatures due to the lengthening of the growing season. Over most regions, where correlations between LAI and SHF are negative, correlations between LAI and LHF are positive. However, in CRCM5_CTEM, the region of eastern Canada, shown in Fig. 8a, stands out. Indeed, in this region, though the LAI-LHF correlations are positive, the LAI-precipitation correlations are mostly non-significant. This leads to the conclusion that vegetation does not suffer from moisture limitation in this region.

For the same region, the correlations between LAI and temperature are positive, though the correlations between LAI and SHF are mostly non-significant. To better understand the interactions, a path analysis is performed to decompose the effect of (1) LAI and SHF on temperature, and (2) LAI and temperature on SHF, as explained in Sect. 2.3 and shown in Fig. 8e, f. The magnitudes of the direct effect of SHF and the indirect effect of LAI (through SHF) on temperature–SHF correlations (Fig. 8e) confirm

that an increase in SHF leads to an increase in temperature. This suggests that the missing link in the LAI–SHF–temperature–LAI interactive loop resides in the correlation between LAI and SHF. Figure 8f shows that the LAI–SHF correlation is non-significant due to the counteracting direct effect of LAI on SHF (−0.25) and indirect effect of temperature on SHF through its effect on LAI (0.22).

3.3.1 Long-term memory

Delire et al. (2011) suggested that the implementation of a dynamic vegetation module in a climate model introduces long-term memory in the system. Indeed, the biosphere is a slow integrator of short-term climate changes, thus influencing the climate in the long-term. To assess the impact of the vegetation memory on the CRCM5 climate, 1-year lagged correlations between the peak LAI and the annual mean precipitation and temperature were calculated, as shown in Fig. 9. For instance, Fig. 9a shows the correlation of precipitation with the LAI when the precipitation leads the LAI by 1 year. Whether looking at the biosphere (LAI) leading the climate or vice versa, CRCM5_CTEM shows significant correlations over many regions compared to CRCM5_STD. The correlations with the precipitation leading the LAI are mostly positive in CRCM5_CTEM over the southwestern parts of North America, since an increase in precipitation benefits vegetation in these regions where water is somewhat a limiting factor to vegetation growth. If the NPP increases during the year with increased precipitation, the LAI will most likely be greater the following year. As can be seen from Fig. 9b, an increase in temperature has a different effect on the vegetation depending on location. In southwest North America where the climate is hot and dry, an increase in temperature leads to heat stress, resulting in a decrease in vegetation live carbon pools and thus in the LAI the following year. In other regions, vegetation benefits from higher temperature since it may lengthen the growing season, thus increasing the vegetation carbon uptake and the LAI the following year. The atmosphere memory relative to the biosphere (Fig. 9c, d) is weaker than the biosphere memory (Fig. 9a, b), which concurs with the observed results from Notaro et al. (2006). However, CRCM5_CTEM indicates that changes in biosphere could lead to significant alterations in the climate in the long-term in sensitive regions, especially since it is the temperature that seems most affected by changes in vegetation coverage, similarly to the findings of Liu et al. (2006).

The results presented above for instantaneous correlations and lead-lag correlations show great resemblance in patterns to those of Notaro et al. (2006) who used observed data in order to study the vegetation-atmosphere feedbacks across the United States. Thus, the model simulation CRCM5_CTEM is consistent with observations and other studies. It was discussed in Sect. 3.2 that CRCM5_CTEM does not clearly improve the model with respect to the mean climate. However, since it introduces biosphere–atmosphere feedbacks and long-term memory in the model, it could be hypothesized that CRCM5_CTEM captures better the variability of biosphere and climate, as it is discussed in the following section.

3.4 Interannual variability and extremes

Several studies have shown that vegetation can dampen or amplify climate variability through changes in vegetation structure and feedbacks (Hughes et al. 2006; Delire et al. 2004, 2011). Thus, in order to study the impact of interactive phenology on the interannual variability of the simulated climate, the coefficient of variation (CV)—defined as the ratio of the standard deviation to mean value—of the seasonal maximum LAI and the seasonal means of LHF, SHF, precipitation, temperature and diurnal temperature range are computed for spring (MAM; Fig. 10) and summer (JJA; Fig. 11), for the 1971–2010 period, for CRCM5_CTEM and CRCM5_STD. CV is used as a measure of variability as it facilitates comparison across variables and seasons.

The interannual variability, quantified in terms of CV, of maximum LAI is clearly higher for CRCM5_CTEM, compared to CRCM5_STD (Figs. 10a, 11a) for both seasons, and is closer to that observed (figure not shown). In spring, the interannual variability of the maximum LAI in CRCM5_STD (Fig. 10a) can be high as it depends on the date of budburst. In summer however (Fig. 11a), the majority of the vegetation has reached its prescribed maximum LAI, except in the high latitudes, where the length of the growing season has a great impact on the maximum LAI. In these high latitude regions, a link can be made with Fig. 8c where the spatial pattern of the correlation between the maximum LAI and mean spring/summer temperature is very similar to the interannual variability of the maximum LAI in summer. As explained previously, this is due to the fact that in CRCM5_STD the phenology of the plants is driven by the 2-m air and the soil temperatures. However, the interannual variability of LAI does not seem to be linked to the interannual variability of the energy fluxes and the climate in CRCM5_STD, which is expected since the maximum LAI is prescribed in CRCM5_STD.

In CRCM5_CTEM, the region of maximum LAI variability shifts from the high-latitude regions in spring to a southerly location, dominated by crops, in summer. For spring, amplification of interannual variability can be noticed for SHF in CRCM5_CTEM, for the same high-latitude regions where higher interannual variability in maximum LAI is noted, which is also reflected in the interannual variability of mean spring temperature (Fig. 10e).

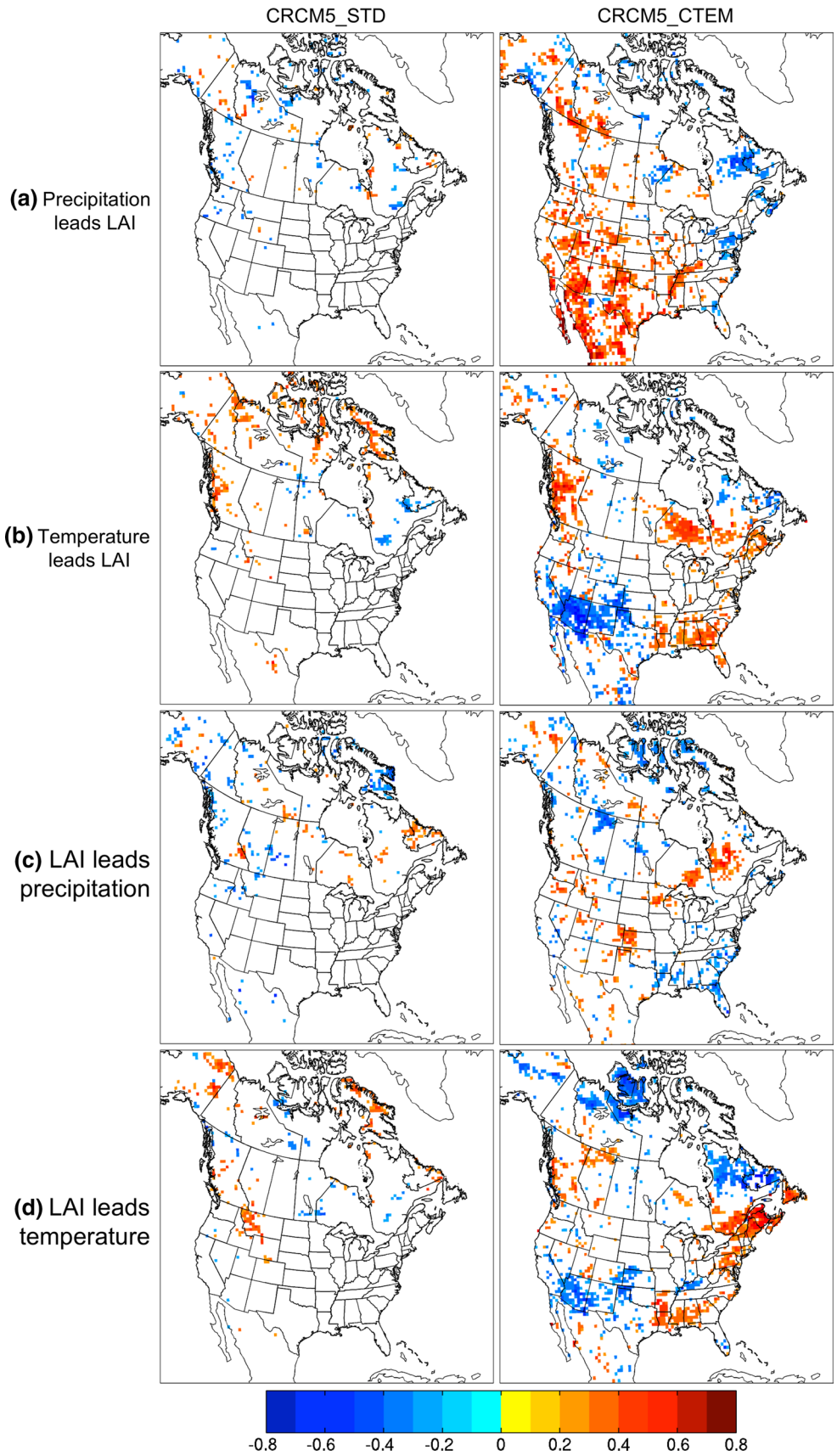

Fig. 9 Spatial plots of 1-year lagged-correlations between **a** precipitation and peak LAI, **b** temperature and peak LAI, **c** peak LAI and precipitation, and **d** peak LAI and temperature, with the first variable leading the second by 1 year in all cases, for CRCM5_STD (column 1) and CRCM5_CTEM (column 2) for the 1971–2010 period. Regions where correlations are not significant are shown in *white*; significance is calculated using the Student's *t* test at 10 % significance level

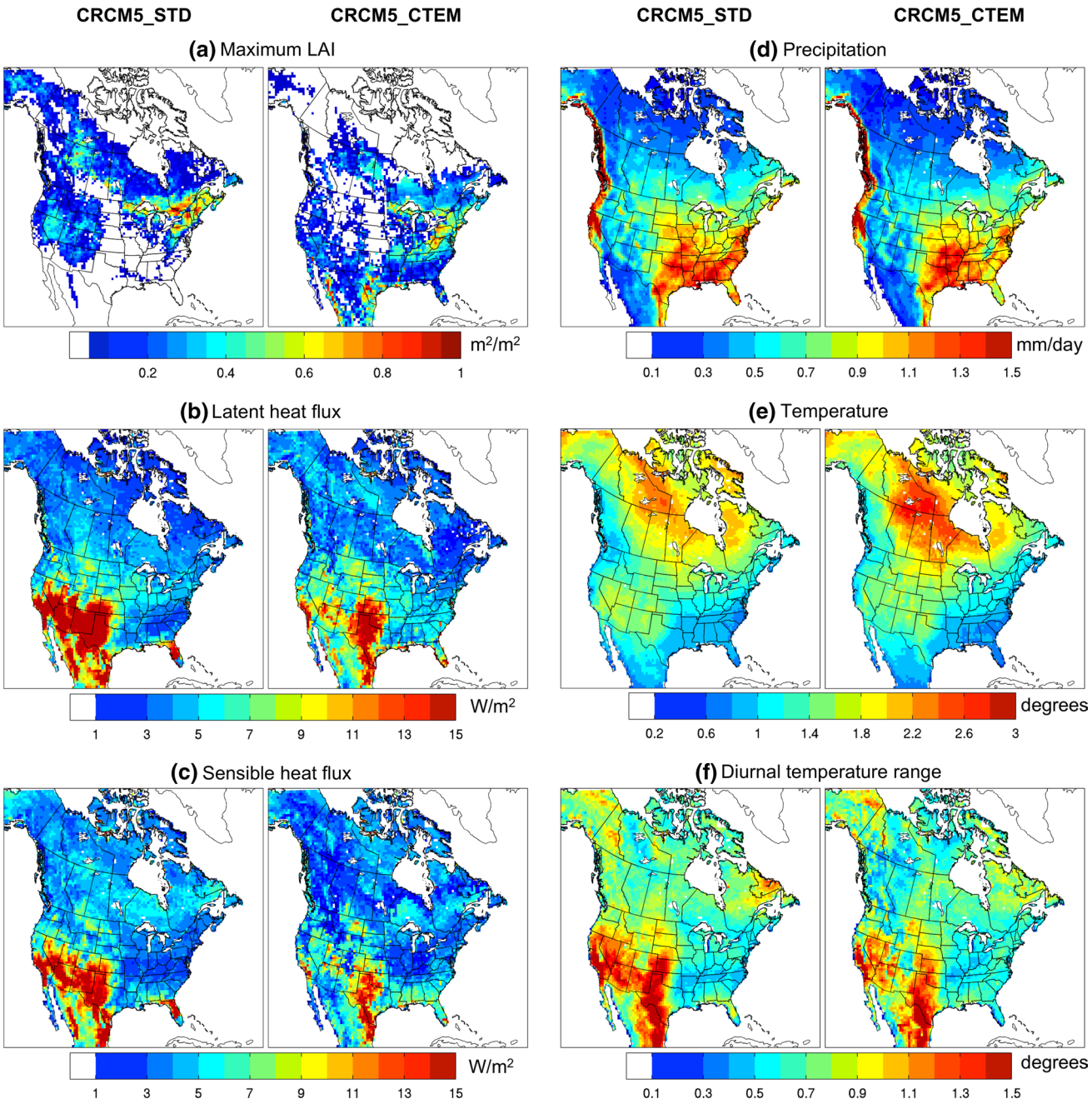

Fig. 10 Spatial plots of the coefficient of variation of the **a** maximum LAI and mean, **b** latent heat flux, **c** sensible heat flux, **d** precipitation, **e** temperature, and **f** diurnal temperature range for the CRCM5_STD and CRCM5_CTEM simulations, for the 1971–2010 period, for spring (MAM) season

The amplification in LHF variability for the same region is much smaller compared to SHF and is expected since the impact of LAI on albedo and therefore on SHF is dominant compared to LHF in these regions.

In spring, despite the higher interannual variability in the southern parts of the domain for maximum LAI in CRCM5_CTEM, a dampening of LHF variability is noted for the southwestern regions of the North American landmass (Fig. 10b) and some amplification in SHF over the central Great Plains (Fig. 10c). The dampened interannual variability in LHF is not reflected in precipitation, as the source of precipitation for these regions is not only related to local recycling of moisture, but also to moist air advected into the region by winds from the adjoining ocean. The impact of the increased interannual variability in SHF for the central Great Plains on the mean temperature is less

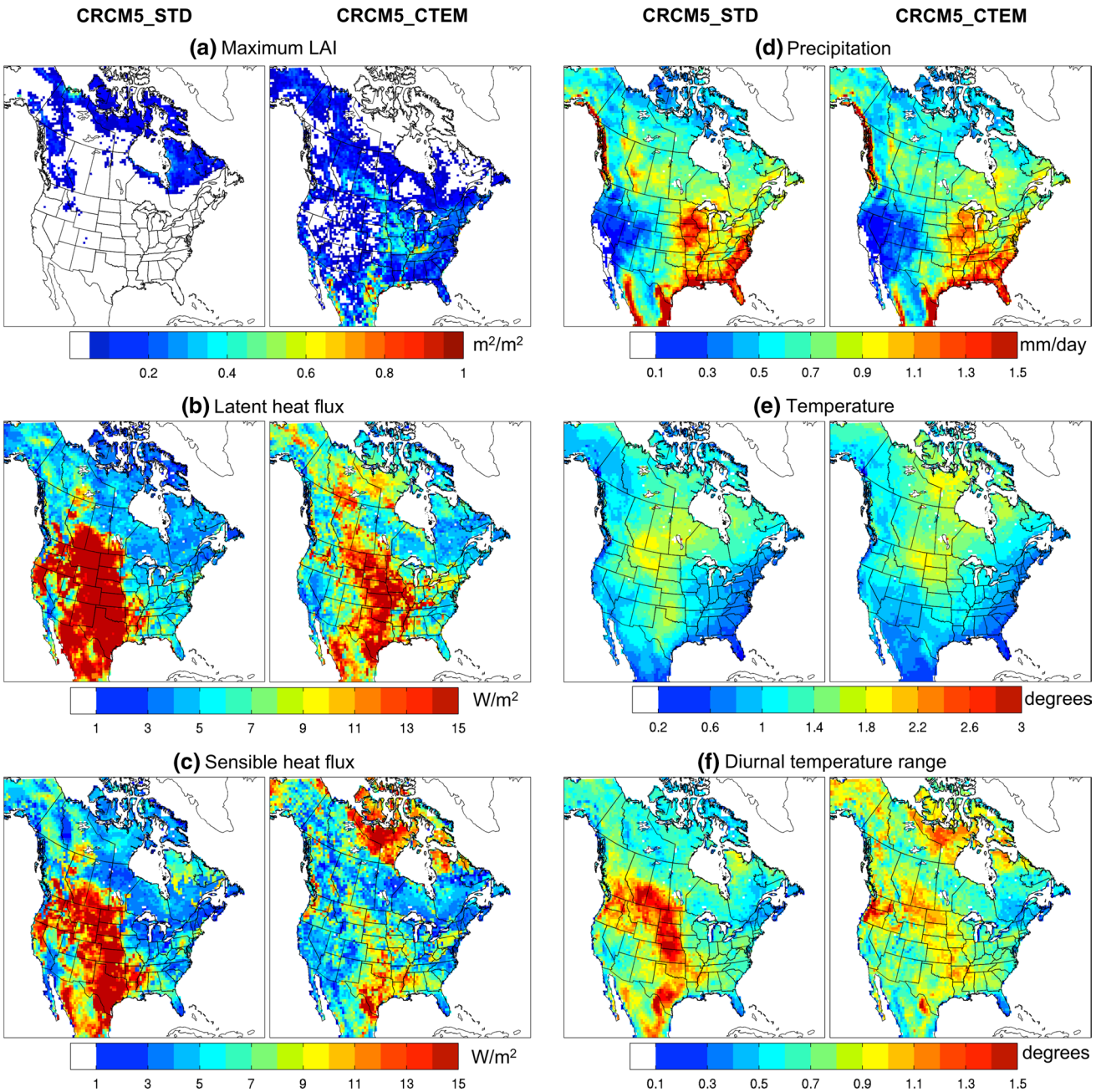

Fig. 11 Spatial plots of the coefficient of variation of the **a** maximum LAI and mean, **b** latent heat flux, **c** sensible heat flux, **d** precipitation, **e** temperature, and **f** diurnal temperature range for the CRCM5_STD and CRCM5_CTEM simulations, for the 1971–2010 period, for summer (JJA) season

evident. As for summer, similar to spring, dampening of LHF variability can be noted in CRCM5_CTEM. Though variability in SHF is higher in high-latitude regions in CRCM5_CTEM in summer compared to CRCM5_STD, no important changes are noticed for other regions.

To investigate further the impact of higher and improved interannual variability of maximum LAI in CRCM5_CTEM on climate, we turn our attention to anomalous dry and wet years. In particular, anomalous dry/wet years over the region with high interannual variability in LAI in summer are selected. For a drought year, we focus on year 1988 when droughts affected east to central parts of central North America, and for an anomalous wet year, we look at year 1993, which affected approximately the same region as the drought of 1988. Figure 12 shows observed (based on Hopkinson et al. (2011) and Maurer et al. (2002) datasets) and CRCM5_CTEM and CRCM5_STD simulated NHD for the summer of 1988. Although the spatial

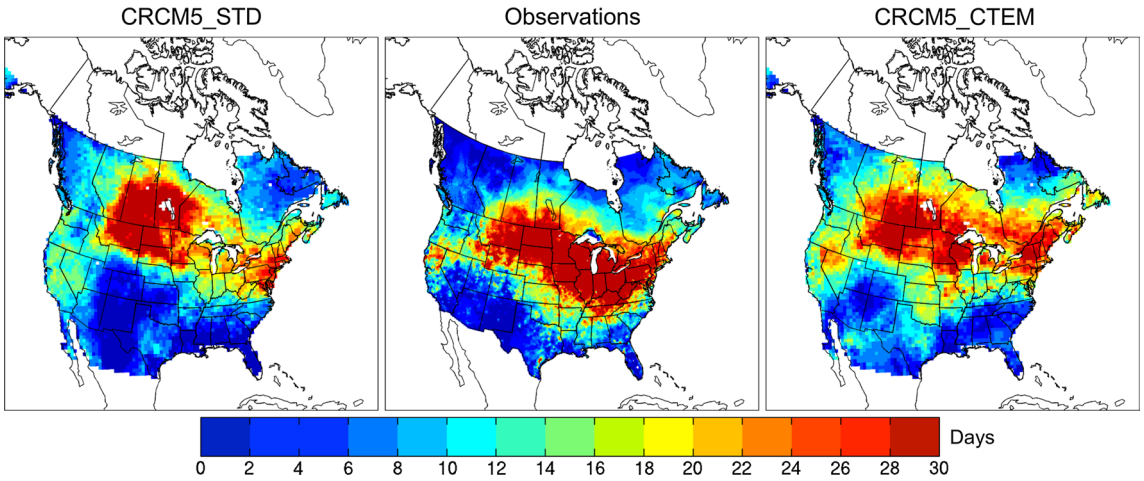

Fig. 12 Number of hot days derived from (*centre*) observed data (Canada: Hopkinson et al. 2011 and USA: Maurer et al. 2002) daily maximum temperature series, and the (*left*) CRCM5_STD and (*right*) CRCM5_CTEM simulations during the summer (JJA) of 1988

pattern of the NHD in CRCM5_CTEM is slightly shifted to the north, the improvement in the simulation of the NHD, compared to CRCM5_STD, is notable. In CRCM5_STD, the NHD is substantially reduced over eastern North America, where the differences in summer LAI (see Fig. 4b) between CRCM5_CTEM and CRCM5_STD are more pronounced, which suggests that a better representation of vegetation cover and the interactions at the land–atmosphere interface leads to better simulation of the NHD.

The impact of the very dry and warm conditions, during the summer of 1988, on the simulated biosphere in CRCM5_CTEM and CRCM_STAT can be assessed from Fig. 13, which shows time series of summer mean values of precipitation, temperature and LAI for the 1971–2010 period, for the drought affected region (between 41°N and 50°N, and 116°W and 88°W). Both simulations capture the 1988 drought, reflected in the below normal precipitation values and the related above normal positive temperatures. The impact of these anomalies on the biosphere is different in CRCM5_STD and CRCM5_CTEM. Indeed, in CRCM5_STD, since precipitation has no direct effect on the LAI, the below normal precipitation apparently has no influence on LAI. On the contrary, the above normal warmer temperature increases the length of the growing season and thus the mean LAI. However, CRCM5_CTEM captures the drought-stress effect on the vegetation. The below normal precipitation leads to water stress, to which the vegetation responds through increased stomatal resistance, thereby reducing the productivity and therefore LAI. Though precipitation picks up and temperature cools in the subsequent years, the LAI continues to drop till 1990 in CRCM5_CTEM, possibly due to the long-term memory of the biosphere and its impact on the atmosphere.

As for the wet summer of 1993, both simulations capture the positive precipitation anomaly, accompanied by anomalously cooler temperatures. Once again, these two climate factors have different effects on the biosphere in the two simulations. In CRCM5_STD, the cooler temperatures in 1993 and 1994 cause the mean LAI to drop, with precipitation having no direct effect on the biosphere. In CRCM5_CTEM however, vegetation benefits from the increased precipitation although this effect is dampened by the cooler temperatures. It should be noted that overly large precipitation, resulting in flooding, could lead to unfavorable conditions for the biosphere, and this is not currently represented in CTEM.

4 Summary and conclusions

The impact of interactive vegetation phenology on CRCM5 simulated climate over North America for the 1971–2010 period is studied by comparing two simulations—CRCM5_STD with prescribed vegetation phenology represented by the land surface scheme CLASS and CRCM5_CTEM which models vegetation phenology as a dynamic component through CTEM coupled with CLASS. Both simulations are driven by ERA-40/ERA-Interim reanalyses at the lateral boundaries.

Comparison of simulated and observed spatial distribution of the biospheric state variable, LAI, suggests that CRCM5_CTEM, particularly in summer, captures better the distribution, except over western Canada where it underestimates the LAI. This bias in the simulated biosphere over western Canada in CRCM5_CTEM could lead to underestimation of biosphere–atmosphere feedbacks, particularly due to the strength of the albedo effect in this region (Loranty et al. 2014), and it could possibly

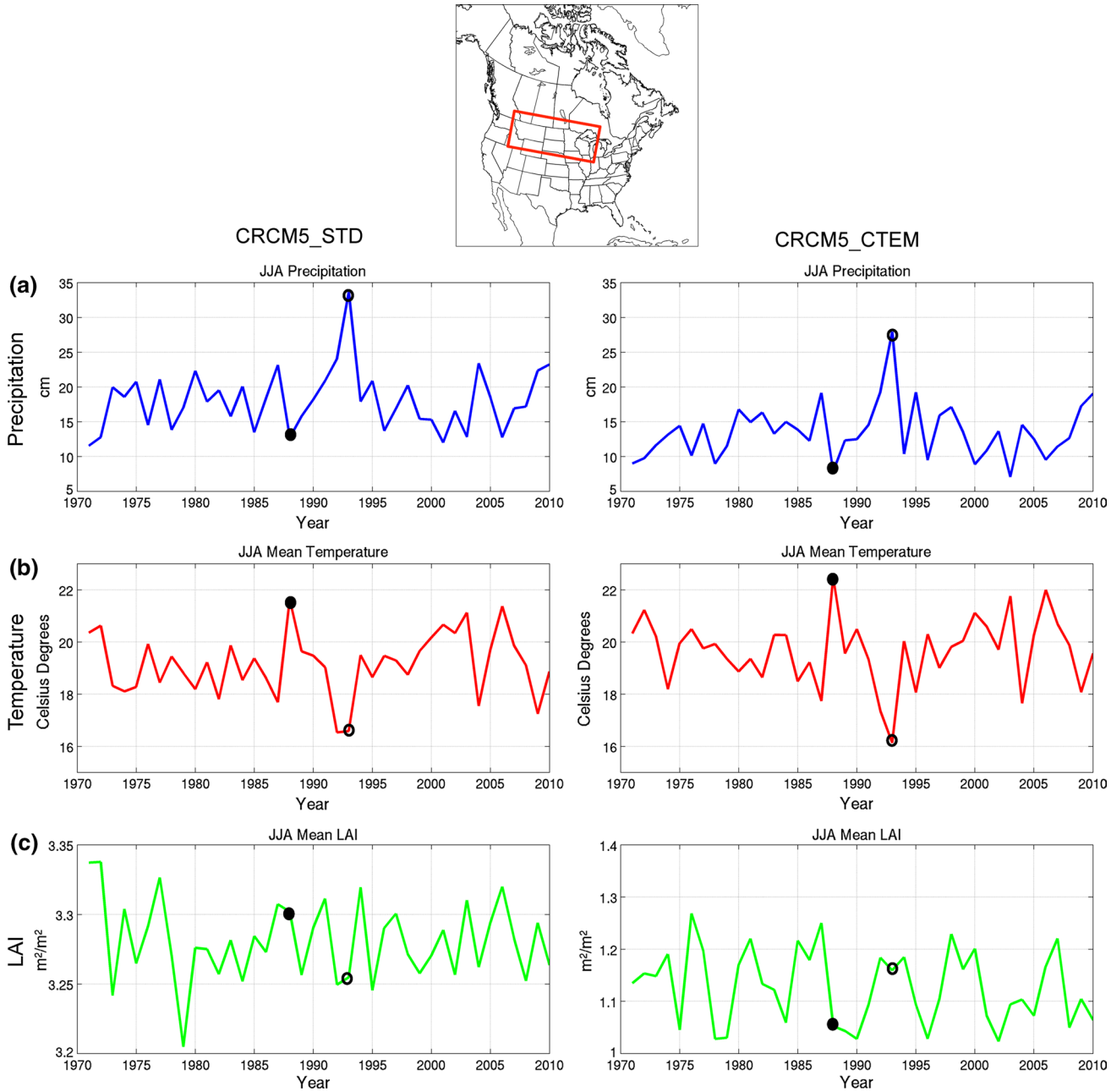

Fig. 13 Evolution of CRCM5_STD (*left column*) and CRCM5_CTEM (*right column*) simulated mean summer **a** precipitation (cm), **b** temperature (°C) and **c** LAI (m^2/m^2; note the different scales on the y-axis) for the 1988 drought affected region (outlined in *red* in the upper plot), for the 1971–2010 period. The *filled* (empty) *circles* correspond to year 1988 (1993)

be rectified by creating a 10th PFT adapted to this region, i.e. a needleleaf evergreen PFT better adapted to drier summers and colder winters through longer leaf life span and lower sensitivity to drought- and cold-stress, as suggested by Peng et al. (2014). It must however be noted that there are big uncertainties in the LAI observation datasets. For example, Gibelin et al. (2006) have shown that the ISLSCP II LAI is higher than other satellite based estimates, especially in the boreal forest.

The differences in LAI, the vegetation characteristic that has the biggest impact on the atmosphere-biosphere interactions, between CRCM5_CTEM and CRCM5_STD lead to differences in surface albedo, SHF and LHF between the two simulations over various regions, which are reflected in the simulated temperature and precipitation fields. In fact, CTEM improves the model (CRCM5) in some regions, although it introduces new biases in other regions such as western USA. Thus the impact of

interactive phenology on the 1971–2010 mean climate can be significant depending on the region and the season. It should be noted that biases in the simulated climate stemming from other sources could influence the simulated vegetation. Garnaud et al. (2014) have shown that the vegetation simulated by CLASS/CTEM is sensitive to the driving climate.

Despite these limitations, the implementation of CTEM in CRCM5 introduces feedbacks between the biosphere and the atmosphere. In fact, the correlations between biospheric and atmospheric variables are significantly stronger in CRCM5_CTEM, particularly with respect to precipitation and surface fluxes. Furthermore, since the biosphere is a slow integrator of short-term climate changes, the implementation of a dynamic vegetation module in a climate model introduces long-term memory in the climate system, thus influencing the climate in the long term, as suggested by Delire et al. (2011) and noted in CRCM5_CTEM. The strongest lagged correlations are between the LAI and temperature, with the average temperature of a given year having a significant impact on the LAI of the following year. Although not as pronounced, the impact of LAI on temperature the following year shows a similar behavior. Once again, this is an indication that CRCM5_CTEM is able to simulate feedback between the biosphere and the climate that could lead to significant alterations in the climate in sensitive regions in the long term. These findings are similar to those obtained by Liu et al. (2006) and Wang et al. (2014) using observations. CRCM5_CTEM simulates better the interannual variability in LAI, which is also reflected in the ability of the model to simulate more realistically the state of the atmosphere and biosphere during anomalously wet and dry years.

This study thus provides important insights on the impact of interactive phenology on the regional climate of North America, particularly related to the variability, both in space and time, in biosphere–atmosphere interactions over the region. As mentioned earlier, this study does not take into account competition between plant functional types. As shown by Smith et al. (2011), competition is important to model vegetation shifts and changing tree line, due to non-negligible effects that this can have on temperature and precipitation feedbacks, particularly in the context of a changing climate. Work is in progress to implement competition in CTEM, and thus future work will focus on the impact of competition on regional climate.

Acknowledgments This project was funded by the Canada Research Chair in Regional Climate Modeling and the Ouranos Consortium. The authors would like to sincerely thank Ms. Katja Winger and Mr. Luis Duarte for their valuable technical assistance.

References

Adam JC, Stephens JC, Chung SH, Brady MP, Evans RD, Kruger CE et al (2014) BioEarth: envisioning and developing a new regional earth system model to inform natural and agricultural resource management. Clim Change 1–17. doi:10.1007/s10584-014-1115-2

Arora VK (2003) Simulating energy and carbon fluxes over winter wheat using coupled land surface and terrestrial ecosystem models. Agric For Meteorol 118(1–2):21–47

Arora VK, Boer GJ (2003) A representation of variable root distribution in dynamic vegetation models. Earth Interact 7(6):1–19

Arora VK, Boer GJ (2005) A parameterization of leaf phenology for the terrestrial ecosystem component of climate models. Glob Change Biol 11:39–59

Arora VK, Boer GJ (2006) Simulating competition and coexistence between plant functional types in a dynamic vegetation model. Earth Interact 10:1–30

Arora VK, Boer GJ (2010) Uncertainties in the 20th century carbon budget associated with land use change. Glob Change Biol 16:3327–3348

Bélair S, Mailhot J, Girard C, Vaillancourt P (2005) Boundary layer and shallow cumulus clouds in a medium-range forecast of a large-scale weather system. Mon Weather Rev 133:1938–1960

Benoit R, Côté J, Mailhot J (1989) Inclusion of a TKE boundary layer parameterization in the Canadian regional finite-element model. Mon Weather Rev 117:1726–1750

Collatz GJ, Ball JT, Grivet C, Berry JA (1991) Physiological and environmental regulation of stomatal conductance, photosynthesis and transpiration: a model that includes a laminar bounadary layer. Agric For Meteorol 54:107–136

Collatz GJ, Ribas-Carbo M, Berry JA (1992) Coupled photosynthesis-stomatal conductance model for leaves of C_4 plants. Aust J Plant Physiol 19:519–538

Côté J, Gravel S, Méthot A, Patoine A, Roch M et al (1998) The Operational CMC-MRB Global Environmental Multiscale (GEM) Model. Part I: design considerations and formulation. Mon Weather Rev 126:1373–1395

Cox P (2001) Description of the "TRIFFID" Dynamic Global Vegetation Model. Hadley Center technical note 24

Dee DP, Uppala SM, Simmons AJ, Berrisford P, Poli P, Kobayashi S, Andrae U, Balmaseda MA, Balsamo G, Bauer P, Bechtold P, Beljaars ACM, van de Berg L, Bidlot J, Bormann N, Delsol C, Dragani R, Fuentes M, Geer AJ, Haimberger L, Healy SB, Hersbach H, Hólm EV, Isaksen L, Kållbergn P, Köhler M, Matricardi M, McNally AP, Monge-Sanz BM, Morcrette J-J, Park B-K, Peubey C, de Rosnay P, Tavolato C, Thépaut J-N, Vitart F (2011) The ERA-Interim reanalysis: configuration and performance of the data assimilation system. Quart J Royal Meteorol Soc 137:553–597. doi:10.1002/qj.828

Delage Y (1997) Parameterising sub-grid scale vertical transport in atmospheric models under statically stable conditions. Boundary Layer Meteorol 82:23–48

Delage Y, Girard C (1992) Stability functions correct at the free convection limit and consistent for both the surface and Ekman layers. Boundary Layer Meteorol 58:19–31

Delire C, Foley JA, Thompson S (2004) Long-term variability in a coupled atmosphere–biosphere model. J Clim 17:3947–3959

Delire C, De Noblet-Ducoudre N, Sima A, Gouirand I (2011) Vegetation dynamics enhancing long-term climate variability confirmed by two models. J Clim 24(9):2238–2257

Dubreuil V, Debortoli N, Funatsu B, Nedelec V, Durieux L (2012) Impact of land-cover change in the Southern Amazonia climate: a case study for the region of Alta Floresta, Mato Grosso, Brazil. Environ Monit Assess 184:877–891

Farquhar GD, von Caemmerer S, Berry JA (1980) A biochemical model of photosynthetic CO2 assimilation in leaves of C_3 species. Planta 149:78–90

Fischer EM, Seneviratne SI, Lüthi D, Schär C (2007) Contribution of land–atmosphere coupling to recent European summer heat waves. Geophys Res Lett 34:L06707. doi:10.1029/2006GL029068

Garnaud C, Sushama L, Arora V (2014) The effect of driving climate data on the simulated terrestrial carbon pools and fluxes. Int J Climatol 34:1098–1110. doi:10.1002/joc.3748

Garrigues S, Lacaze R, Baret F, Morisette JT, Weiss M, Nickeson JE, Fernandes R, Plummer S, Shabanov NV, Myneni RB, Knyazikhin Y, Yang W (2008) Validation and intercomparison of global Leaf Area Index products derived from remote sensing data. J Geophys Res 113. doi:10.1029/2007JG000635

Gibelin A-L, Calvet J-C, Roujean J-L, Jarlan L, Los SO (2006) Ability of the land surface model ISBA-A-gs to simulate leaf area index at the global scale: Comparison with satellites products. J Geophys Res 111. doi:10.1029/2005JD006691

Hall FG, Brown de Colstoun E, Collatz GJ, Landis D, Dirmeyer P, Betts A, Huffman G, Bounoua L, Meeson B (2006) The ISLSCP initiative II global data sets: surface boundary conditions and atmospheric forcings for land–atmosphere studies. J Geophys Res 111. doi:10.1029/2006JD007366

Hansen J, Sato M (2001) Trends of measured climate forcing agents. Proc Natl Acad Sci USA 98:14778–14783

Hansen J, Sato M (2004) Greenhouse gas growth rates. Proc Natl Acad Sci USA 101:16109–16114

Hopkinson RF, McKenney DW, Milewska EJ, Hutchinson MF, Papadopol P, Vincent LA (2011) Impact of aligning climatological day on gridding daily maximum-minimum temperature and precipitation over Canada. J Appl Meteorol Climatol 50(8):1654–1665

Hughes JK, Vlades PJ, Betts R (2006) Dynamics of a global-scale vegetation model. Ecol Model 198:452–462

Kain JS, Fritsch JM (1990) A one-dimensional entraining/detraining plume model and application in convective parameterization. J Atmos Sci 47:2784–2802

Klein Goldewijk K (2001) Estimating global land use change over the past 300 years: the HYDE Database. Global Biogeochem Cycles 15:417–433

Kraucunas I, Clarke L, Dirks J, Hathaway J, Hejazi M, Hibbard K et al (2014) Investigating the nexus of climate, energy, water, and land at decision-relevant scales: the Platform for Regional Integrated Modeling and Analysis (PRIMA). Clim Change 1–16. doi:10.1007/s10584-014-1064-9

Kuo HL (1965) On formation and intensification of tropical cyclones through latent heat release by cumulus convection. J Atmos Sci 22:40–63

Laprise R (1992) The Euler equation of motion with hydrostatic pressure as independent coordinate. Mon Weather Rev 120(1):197–207

Li R, Arora VK (2011) Effect of mosaic representation of vegetation in land surface schemes on simulated energy and carbon balances. Biogeosciences Discuss 8:5849–5879

Li J, Barker HW (2005) A radiation algorithm with correlated-k distribution. Part I: local thermal equilibrium. J Atmos Sci 62:286–309

Liu Z, Notaro M, Kutzbach J (2006) Assessing global vegetation-climate feedbacks from observations. J Clim 19:787–814

Loranty MM, Berner LT, Goetz SJ, Jin Y, Randerson JT (2014) Vegetation controls on northern high latitude snow-albedo feedback: observations and CMIP5 model simulations. Glob Change Biol 20:594–606. doi:10.1111/gcb.12391

Los SO, Collatz GJ, Sellers PJ, Malmström CM, Pollack NH, DeFries RS, Bounoua L, Parris MT, Tucker CJ, Dazlich DA (2000) A global 9-year biophysical land-surface data set from NOAA AVHRR data. J Hydrometeor 1:183–199. doi:10.1175/1525-7541(2000)001<0183:AGYBLS>2.0.CO;2

Martynov A, Laprise R, Sushama L, Winger K, Separovic L, Dugas B (2013) Reanalysis-driven climate simulation over CORDEX North America domain using the Canadian regional Climate Model, version 5: model performance evaluation. Clim Dyn 41:2973–3005. doi:10.1007/s00382-013-1778-9

Maurer EP, Wood AW, Adam JC, Lettenmaier DP, Nijssen B (2002) A long-term hydrologically-based data set of land surface fluxes and states for the conterminous United States. J. Climate 15:3237–3251

McFarlane NA (1987) The effect of orographically excited gravity-wave drag on the circulation of the lower stratosphere and troposphere. J Atmos Sci 44:1175–1800

Mitchell TD, Jones PD (2005) An improved method of constructing a database of monthly climate observations and associated high-resolution grids. Int J Climatol 25:693–712. doi:10.1002/joc.1181

Notaro M, Liu Z, Williams JW (2006) Observed vegetation-climate feedbacks in the United States. J Clim 19:763–786

Notaro M, Vavrus S, Liu Z (2007) Global vegetation and climate change due to future increases in CO_2 as projected by a fully coupled model with dynamic vegetation. J Clim 20:70–90

Peng C (2000) From static biogeographical model to dynamic global vegetation model: a global perspective on modelling vegetation dynamics. Ecol Model 135:33–54

Peng Y, Arora VK, Kurz WA, Hember RA, Hawkins BJ, Fyfe JC, Werner AT (2014) Climate and atmospheric drivers of historical terrestrial carbon uptake in the province of British Columbia, Canada. Biogeosciences 11:635–649

Pielke RA, Avissar R Sr, Raupach M, Dolman AJ, Zeng X, Denning AS (1998) Interactions between the atmosphere and terrestrial ecosystems: influence on weather and climate. Glob Change Biol 4:461–475

Pinto E, Shin Y, Cowling SA, Jones CD (2009) Past, present and future vegetation-cloud feedbacks in the Amazon Basin. Clim Dyn 32(6):741–751

Prentice IC et al (1992) A global biome model based on plant physiology and dominance, soil properties and climate. J Biogeogr 19(2):117–134

Quillet A, Peng C, Garneau M (2010) Toward dynamic global vegetation models for simulating vegetation-climate interactions and feedbacks: recent developments, limitations and future challenges. Environ Rev 18:333–353

Schulze ED, Leuning R, Kelliher FM (1995) Environmental regulation of surface conductance for evaporation from vegetation. Vegetation 121:79–87

Sietse OL (2010) ISLSCP II FASIR-adjusted NDVI Biophysical Parameter Fields, 1982–1998. In: Hall FG, Collatz G, Meeson B, Los S, Brown de Colstoun E, Landis D (eds) ISLSCP Initiative II Collection. Data set. Available on-line [http://daac.ornl.gov/] from Oak Ridge National Laboratory Distributed Active Archive Center, Oak Ridge, Tennessee, U.S.A. doi:10.3334/ORNLDAAC/972

Smith B, Prentice IC, Sykes MT (2001) Representation of vegetation dynamics in the modelling of European ecosystems: Comparison of two contrasting approaches. Global Ecol Biogeogr 10:621–637. doi:10.1046/j.1466-822X.2001.00256.x

Smith B, Samuelsson P, Wramneby A, Rummukainen M (2011) A model of the coupled dynamics of climate, vegetation and

terrestrial ecosystem biogeochemistry for regional applications. Tellus 63A:87–106

Snyder PK, Foley JA, Hitchman MH, Delire C (2004) Analyzing the effects of complete tropical forest removal on the regional climate using a detailed three-dimensional energy budget: An application to Africa. J Geophys Res 109:D21102. doi:10.1029/2003JD004462

Stéfanon M, Drobinski P, D'Andrea F, de Nolet-Ducoudré N (2012) Effect of interactive vegetation phenology on the 2003 summer heat waves. J Geophys Res 117:D24103. doi:10.1029/2012JD018187

Stephenson NL (1990) Climatic control of vegetation distribution: the role of the water balance. Am Nat 135:649–670

Sundqvist H, Berge E, Kristjansson JE (1989) Condensation and cloud parameterization studies with a mesoscale numerical weather prediction model. Mon Weather Rev 117:1641–1657

Taylor KE, Williamson DL, Zwiers FW (2000) The sea surface temperature and sea-ice concentration boundary conditions for AMIP II simulations. Program for Climate Model Diagnosis and Intercomparison, Lawrence Livermore National Laboratory, p 25

Uppala SM et al (2005) The ERA-40 re-analysis. Quart J Royal Meteorol Soc 131(612):2961–3012

Van den Hoof C, Hanert E, Vidale PL (2011) Simulating dynamic crop growth with an adapted land surface model- JULES-SUCROS: Model development and validation. Agric For Meteorol 151:137–153

Verseghy DL (1991) CLASS - A Canadian land surface scheme for GCMs, I Soil model. Int J Climatol 11:111–133

Verseghy DL (2011) CLASS—The Canadian land surface scheme (version 3.5). Technical Documentation (version 1). Environment Canada, Climate research division, Science and Technology branch

Verseghy DL, McFarlane NA, Lazare M (1993) CLASS—A Canadian land surface scheme for GCMs, II. Vegetation model and coupled runs. Int J Climatol 13:347–370

Wang A, Price D, Arora V (2006) Estimating changes in global vegetation cover (1850–2100) for use in climate models. Global Biogeochem Cycles 20(3):GB3028.1–GB3028.15

Wang F, Notaro M, Liu Z, Chen G (2014) Observed local and emote influences of vegetation on the atmosphere across North America using a model-validated statistical technique that first excludes oceanic forcings. J Clim 27:362–382

Webb RS, Rosenzweig CE, Levine ER (1991) A global data set of soil particle size properties. NASA Technical Memorandum, 4286

Willmott CJ, Matsuura K (1995) Smart interpolation of annually averaged air temperature in the United States. J App Meteorol 34:2577–2586

Woodward FI (1987) Climate and plant distribution. Cambridge University Press, Cambridge, p 174

Wramneby A, Smith B, Samuelsson P (2010) Hot spots of vegetation-climate feedbacks under future greenhouse forcing in Europe. J Geophys Res 115:D21119. doi:10.1029/2010JD014307

Yeh K-S, Côté J, Gravel S, Méthot A, Patoine A et al (2002) The CMC-MRB global environmental multiscale (GEM) model. Part III: nonhydrostatic formulation. Mon Weather Rev 130:339–356

Zadra A, Roch M, Laroche S, Charron M (2003) The subgrid scale orographic blocking parametrization of the GEM model. Atmos Ocean 41:155–170

Zadra A, Caya D, Côté J, Dugas B, Jones C et al (2008) The next Canadian Regional Climate Model. Phys Can 64(2):75–83

Zhao X, Tan K, Zhao S, Fang J (2011) Changing climate affects vegetation growth in the arid region. J Arid Environ 75:946–952